Non-Debye heat capacity formula refined and applied to GaP, GaAs, GaSb, InP, InAs, and InSb

Cite as: AIP Advances **3**, 082108 (2013); https://doi.org/10.1063/1.4818273
Submitted: 12 April 2013 • Accepted: 30 July 2013 • Published Online: 06 August 2013

R. Pässler

AIP ADVANCES **3**, 082108 (2013)

Non-Debye heat capacity formula refined and applied to GaP, GaAs, GaSb, InP, InAs, and InSb

R. Pässler[a]
Technische Universität Chemnitz, Institut für Physik, D-09107 Chemnitz, Germany

(Received 12 April 2013; accepted 30 July 2013; published online 6 August 2013)

Characteristic non-Debye behaviors of low-temperature heat capacities of GaP, GaAs, GaSb, InP, InAs, and InSb, which are manifested above all in form of non-monotonic behaviors (local maxima) of the respective $C_p(T)/T^3$ curves in the cryogenic region, are described by means of a refined version of a recently proposed low-to-high-temperature interpolation formula of non-Debye type. Least-mean-square fittings of representative $C_p(T)$ data sets available for these materials from several sources show excellent agreements, from the liquid-helium region up to room temperature. The results of detailed calculations of the respective material-specific Debye temperature curves, $\Theta_D(T)$, are represented in graphical form. The strong, non-monotonic variations of $\Theta_D(T)$ values confirm that it is impossible to provide reasonable numerical simulations of measured $C_p(T)$ dependences in terms of fixed Debye temperatures. We show that it is possible to describe in good approximation the complete Debye temperature curves, from the cryogenic region up to their definitive disappearance (dropping to 0) in the high temperature region, by a couple of unprecedented algebraic formulas. The task of constructing physically adequate prolongations of the low-temperature $C_p(T)$ curves up to melting points was strongly impeded by partly rather large differences (up to an order of 10 J/(K · mol)) between the high-temperature data sets presented in different research papers and/or data reviews. Physically plausible criteria are invoked, which enabled an a priori rejection of a series of obviously unrealistic high-temperature data sets. Residual uncertainties for GaAs and InAs could be overcome by re-evaluations of former enthalpy data on the basis of a novel set of properly specified four-parameter polynomial expressions applying to large regions, from moderately low temperatures up to melting points. Detailed analytical and numerical descriptions are given for the anharmonicity-related differences of isobaric vs. isochoric (harmonic) parts of heat capacities. Relevant sets of empirical parameters and representative collections of heat capacity and Debye temperature values for all materials under study are presented in tabulated form. [http://dx.doi.org/10.1063/1.4818273]

I. INTRODUCTION

The temperature dependences of isobaric heat capacities are playing a key role in thermodynamics of solids. Detailed numerical information on the individual material-specific $C_p(T)$ values, from cryogenic up to high temperatures, is the prerequisite for calculating the respective standard thermodynamic functions like entropies, $S_p(T)$, and enthalpies, $H_p(T)$. The experimental basis for such thermodynamic descriptions is usually given in form of tables and/or graphical representations of measured (or estimated) $C_p(T)$ data points, which have been presented, for a large variety of solids, in numerous thermo-physical and -chemical research papers. More or less representative collections of genuine low-temperature $C_p(T)$ data sets ($0 < T <$300 K) are available, among other

[a]Electronic address: passler@physik.tu-chemnitz.de. Phone: +49 (0)371 531 33208; Fax: +49 (0)371 531 21009

things, from various thermo-physical data collections.[1–3] Concerning the adjacent high-temperature region ($T \geq 298.15$ K), one may refer to collections of $C_p(T)$ tables that are given for an enormous variety of materials in several thermo-chemical data reviews.[4–6] Unfortunately, the selected $C_p(T)$ values listed within the latter reviews are not representing direct results of genuine heat capacity measurements. Instead, these $C_p(T)$ values are quantifying the outcomes of various preliminary fitting and smoothing procedures that are as a rule based on relatively simple analytical expressions (polynomials) for enthalpies, $H_p(T)$, and the respective heat capacities, $C_p(T) = dH_p(T)/dT$. Most frequently used in this connection is the well-known Maier-Kelley equation,[7,8]

$$C_p(T) = a + bT - cT^{-2}, \tag{1}$$

where the three empirical parameters, a, b, and c, are as a rule positive. This simple trinomial equation has been used in particular in a series of thermo-chemical research papers[9–17] for rough simulations of more or less uncertain $C_p(T > 300K)$ data sets available for various III-V materials. The physical origin of the linear term occurring in this equation is commonly ascribed to lattice anharmonicity and expansion effects, which are usually the dominating causes of the temperature dependences observable at high temperatures. However, in various cases, the $C_p(T)$ dependences close to the melting points show a more or less pronounced non-linear (concave) behavior, the simulation of which requires at least an incorporation of an additional quadratic term into Eq. (1) (see some exemplifications in Refs. 4 and 18). In contrast to this, in various publications, one is even concerned with arbitrary omissions of the genuine non-linear term ($\propto T^{-2}$) in Eq. (1). This corresponds to a reduction of the Maier-Kelley equation to an exclusively linear dependence, $C_p(T) \to a + bT$. (See the linear sequences of $C_p(T)$ values given e. g. for GaP in Ref. 4 for GaAs and InAs in Refs. 4 to 6, 19, and 20, for GaSb in Refs. 4, 6, and 21, for InP in Refs. 4 and 5, and for InSb in Refs. 4 and 21.) It is obvious that such an unfounded linearization of the whole high-temperature $C_p(T)$ curves, beginning from the commonly considered thermo-chemical reference temperature, $T_r \equiv 298.15$ K, up to melting points (T_m), represents an excessive simplification of the true state of affairs. Especially grave is the circumstance that the differences between estimated $C_p(T_m)$ values due to linear approximations by different authors can reach in certain cases even an order of 10% (e. g. for GaAs and InAs; see Sec. III).

Fortunately, much more reliable and largely accurate are the thermo-physical $C_p(T < T_r)$ data sets which are available from numerous research papers published since the middle of the past century. The comparatively high quality of thermo-physical data sets is due to the circumstance that the corresponding low-temperature $C_p(T)$ measurements have been usually performed by the adiabatic calorimetry method, the possible uncertainties of which are as a rule limited to magnitudes smaller than 0.5%. The comparatively high degree of reliability of most $C_p(T < T_r)$ data sets is confirmed, among other things, by the usual compatibility (approximate equality) of the data published for one and the same material by different authors (cf. Sec. III).

On the other hand, just the relatively high quality of many thermo-physical data sets represented already for decades a permanent challenge for trying to devise adequate analytical models, which should be capable of providing fine numerical simulations of the $C_p(T)$ data sets in question, from the cryogenic region up to the room temperature region (at least). The earliest attempts in this direction are well known from the pioneering papers by Einstein,[22] who reduced the phonon spectrum in roughest approximation to a single lattice oscillator, and by Debye,[23] who approximated the phonon density of states (PDOS) spectra simply by a quadratic function. The well-known advantage of the latter was its capability of giving a physical plausible explanation of the occurrence of cubic asymptotes for isochoric (including isobaric) lattice heat capacities in the $T \to 0$ limit, $C_{V/p}(T) \propto T^3$ (cf. Refs. 24 to 27). However, numerous careful studies of the actual cryogenic $C_{V/p}(T)$ dependences, like those performed already years ago for alkali halides,[28–30] MgO,[31] and several III-V materials,[32] have shown that strong deviations from this asymptotic behavior are as a rule occurring even within the liquid-helium-hydrogen region. Consequently, it is generally impossible to describe measured $C_p(T)$ dependences by means of the original Debye function[23] involving an unambiguously fixed Debye temperature, Θ_D (whichever its actual value would be). This general breakdown of Debye's original model, just within the cryogenic region, is manifested in particular by the commonly observed non-monotonic (local maximum) behaviors of the associated

$C_{V/p}(T)/T^3$ curves for elemental group-IV materials,[33–35] for GaN,[36,37] as well as for a variety of II-VI materials[37–44] (see also the analogous, non-monotonic $C_{V/p}(T)/T^3$ curves which are shown in Sec. III for the III-V materials under study). In contrast to these numerous experimental observation, the fictitious $C_D(T)/T^3$ model curves due to Debye's original $C_D(T)$ function,[23–27]

$$\frac{C_D(T)}{T^3} = \frac{3}{\Theta_D^3} \int_0^{\Theta_D/T} dx \frac{x^4 e^x}{(e^x-1)^2}, \tag{2}$$

show a plateau behavior[45] in the $T \to 0$ limit, $C_D(T)/T^3 \to (12/5)\pi^4 n_A R/\Theta_D^3$ (from 0 up to about $\Theta_D/12$), which is followed by a monotonic decrease, at increasing temperature (i. e. in general $d(C_D(T)/T^3)/dT < 0$; cf. the insets to the figures presented in Sec. III). Accordingly, among the hitherto known empirical $C_{V/p}(T)/T^3$ curves, such a Debye-model-like behavior (2) has never been observed. An apparently practicable way out of this dilemma, which had been frequently adopted in the past, consisted in an admission of the inherently contradictory concept of certain T-dependent (effective) Debye temperatures, $\Theta_D(T)$. The latter have naturally been found, for elemental group-IV materials,[46–50] as well as for a large variety of binary III-V materials,[51–62] to change as a rule very strongly (and mostly in non-monotonic way) with increasing temperature (see also Sec. IV).

In order to overcome this largely unsatisfactory state of affairs of the conventional heat capacity theory, various authors have suggested more or less simple hybrid models.[63–73] These models were as a rule basing on applications of a Debye-like expression[23] exclusively to the heat capacity contributions of the 3 acoustic (TA and LA) phonon branches, whereas the remaining set of optical (TO and LO) phonon branches was represented by discrete lattice oscillators of Einstein type[22] (only a single one in several cases).[68–70] Hybrid models of this type are, from physical points of view, somewhat more realistic than their grossly oversimplified predecessors proposed by Einstein[22] and Debye.[23] Nevertheless, due to the persistent ignorance of the inherent non-Debye character of the low-temperature contributions made mainly by the TA phonon peaks, the aforementioned hybrid models were, again, incapable of accounting for the commonly observed non-monotonic (local maximum) behaviors of $C_{V/p}(T)/T^3$ curves in the cryogenic region.

A decisive improvement in the latter respect has been achieved only recently owing to the unconventional representation of the contributions of both the TA and the LA peaks by separate Einstein oscillators, in combination with a rigorous cut of the quadratic PDOS spectral components (of Debye type) just at the first TA peak.[43,50,74] (Note that the rigorous limitation of any continuous components of PDOS model functions just by the lowest TA peaks is also in qualitative accordance with an early idea for constructing physically reasonable hybrid model functions by Baron and Morrison.)[30] Such finer subdivisions of the acoustical parts of PDOS spectral functions imply, of course, an enlargement of the total set of discrete, model-specific oscillators, the effective positions and relative weights of which have to be adjusted in the course of subsequent least-mean-square processes. The corresponding fitting procedures are sometimes not easy to perform, especially in cases of binary materials with hexagonal structure, as well as for a wealth of ternary materials, owing to relatively large numbers ($\geq$9) of optical phonon branches. In such cases one is concerned with the notorious problem of pre-selecting an apparently adequate grouping[73,75] of the numerous optical branches into a significantly smaller number of compound (effective) Einstein peaks.

In view of such effective oscillator constellation ambiguities, which are inherent to applications of any multi-oscillator hybrid model to materials with many optical phonon branches, an alternative fitting model might be welcome whose analytical structure is independent of structural details of PDOS spectra. The prototype of a duly global analytical model which is, among other things, completely free from any numerical integration procedure, has been presented in a recent paper[37] in form of a characteristic non-Debye heat capacity interpolation formula (see Eq. (A1), in Appendix A). It was already shown in Ref. 37, for GaN[36] and ZnO,[39,76] that this formula is capable of providing good numerical simulations of the non-monotonic (local maximum) behaviors of the corresponding $C_p(T)/T^3$ curves in the cryogenic region.

We have performed here, in the Appendix A, a convenient transformation (parameter re-definition) of the preceding non-Debye formula,[37] in combination with a further refinement of

its analytical structure. A brief sketch of the whole analytical framework which will actually be used within the present paper is given in Sec. II. Corresponding least-mean-square fittings of combined (mutually compatible) sets of low- and high-temperature $C_p(T)$ data, that are available for a series of cubic III-V materials (GaP, GaAs, GaSb, InP, InAs, and InSb) are performed in Sec. III. For the sake of comparisons with various former (partial) results[51–62] for T-dependent Debye temperature curves we have performed in Sec. IV the corresponding transformations of the relevant sections of fitted $C_p(T)$ curves into the conventional effective Debye temperature representation. The strong non-monotonic T-dependences of the corresponding $\Theta_D(T)$ curves give a clear picture of the pronounced non-Debye character of the heat capacity properties for all materials under study. A detailed discussion of present results is given in Sec. V.

II. BASIC EQUATIONS OF THE NON-DEBYE HEAT CAPACITY MODEL DESCRIPTION

Within the frame of the harmonic regime, the temperature dependences of isochoric heat capacities per mol, $C_{Vh}(T)$, are generally limited by an upper boundary, $C_{Vh}(T \to \infty)$, corresponding to the classical Dulong-Petit value,

$$C_{Vh}(T) = 3n_A R\kappa_P(T) \le 3n_A R = C_{Vh}(\infty), \tag{3}$$

where R is the gas constant, n_A is the number of atoms per molecule of the material in question (i. e. here $n_A = 2$, for the binary III-V materials under study), and $0 \le \kappa_P(T) \le \kappa_P(\infty) = 1$ is a material-specific heat capacity shape function. The latter is known to be generally given by an integral of the form[43,50,74,77–82]

$$\kappa_P(T) = \int d\varepsilon g_P(\varepsilon) \left(\frac{\varepsilon}{2k_B T} \Big/ \sinh\left(\frac{\varepsilon}{2k_B T} \right) \right)^2 \Big/ \int d\varepsilon g_P(\varepsilon), \tag{4}$$

where $g_P(\varepsilon \equiv \hbar\omega)$ represents the phonon density of states spectral function.[24,48,77–79,83,84] Fortunately, even without having detailed numerical information on the actual PDOS spectrum, $g_P(\varepsilon)$, it is possible to derive from Eq. (4) some general analytical expressions, at least for limiting regions of high and low temperatures.

Concerning the behavior of $\kappa_P(T)$ at high temperatures, it follows from Thirring's expansion[85] that the $\kappa_P(T)$ curves are tending to unity via close approaches to the respective high-temperature asymptotes,[24,65,82,85]

$$\kappa_P(T) \to 1 - \frac{\mu_P^{(2)}}{12(k_B T)^2} + ..., \tag{5}$$

where $\mu_P^{(2)}$ represents the second moment of the PDOS spectrum. On the other hand, the limiting behavior of $\kappa_P(T)$ in the cryogenic region is determined by the low-energy tail behaviors of PDOS spectra. These are known to be generally represented by even-order Taylor series expansions,[29,45,47,50] $g_P(\varepsilon) = \gamma_2\varepsilon^2 + \gamma_4\varepsilon^4 + \gamma_6\varepsilon^6 + ...$, the expansion coefficients of which are throughout positive. This expansion involves, according to Eq. (4) (in combination with Eq. (3)), low-temperature behaviors of harmonic lattice heat capacities in form of truncated odd-order Taylor series expansions,[29,31,32,45,47,86–88]

$$C_{Vh}(T) \to c_3 T^3 + c_5 T^5 + c_7 T^7. \tag{6}$$

The expansion coefficient for the cubic term, c_3, is well known to be connected with the $T \to 0$ limiting value,[23,24,45] $\Theta_D(0)$, of the Debye temperature by the relation

$$c_3 = (12/5)\pi^4 n_A R/(\Theta_D(0))^3, \tag{7}$$

(in accordance with Eq. (2)). However, it is continually found within numerical applications to low-temperature tails of cryogenic $C_{V/p}(T)$ data sets that the range of validity of the simple trinomial odd-order power expansion (6) is limited to very narrow intervals,[29,45] $0 \le T < \Theta_D(0)/30$. This means, for many materials, an applicability of Eq. (6) merely to the lower part of the liquid-helium-hydrogen region.[45] At the same time it is usually found that the expansion coefficients for the

two higher-order power terms, T^5 and T^7, are positive, $c_5 > 0$ and $c_7 > 0$.[29,45] Consequently, the respective low-temperature tails of $C_{V/p}(T)/T^3$ curves,

$$C_{V/p}(T)/T^3 \to c_3 + c_5 T^2 + c_7 T^4, \tag{8}$$

are monotonically increasing. This basic low-temperature property is, naturally, in striking contrast to Debye's theoretical model[23] (cf. Eq. (2)). The occurrence of the two positive higher-order terms is the reason why it is throughout impossible,[45] even within the liquid-helium-hydrogen region, to properly simulate the T-dependences of measured lattice heat capacities by means of Debye's original $C_D(T)$ formula,[23] at fixed $\Theta_D \to \Theta_D(0)$. (Concerning some contemporary papers, the authors of which are nevertheless still adhering to the illusionary idea of simulating various $C_p(T)$ data sets by using merely quite accurately calculated Debye functions[23] with constant Θ_D values, see e. g. Refs. 89 and 90).

The temperature dependences of $C_{Vh}(T) \propto \kappa_P(T)$ functions that are resulting from numerical calculations via Eq. (4) show automatically correct high- and low-temperature limiting behaviors (in accordance with (5) and (6), respectively), provided that physically adequate expressions for the underlying PDOS spectral functions have been used. Such usable $g_P(\varepsilon)$ functions may be given either in form of duly detailed graphs (or tables) resulting from material-specific first principles calculations[36,41,42,44] or in form of properly devised multi-oscillator hybrid model functions.[43,50,74] Any one of these two alternative calculation procedures for $C_{Vh}(T)$ curves, however, requires more or less comprehensive pieces of information on microscopic (quantum-mechanical) properties of the material in question. This circumstance raised the question whether, and in which way, it might be possible to devise a usable analytical framework of purely thermodynamic type, which does not involve one or the other piece of information on microscopic properties. An exemplary solution of this problem has recently been presented[37] in terms of a certain 7-parameter interpolation formula for $C_{Vh}(T)$ curves (see Eq. (A1), in the Appendix A). For forthcoming applications it is useful, however, to perform still a convenient transformation of Eq. (A1) in order to be able to rewrite this semi-empirical $C_{Vh}(T)$ function (in analogy to (3)) in form of a product (Eq. (A2)) of the classical Dulong-Petit limiting value, $C_{Vh}(\infty) = 3n_A R$ (3), with a corresponding (normalized) shape function, $\kappa_P(T)$ (Eq. (A3)). Within the frame of present numerical simulations of the heat capacity data sets under study (in see Sec. III) we have found, among other things, that marked refinements of the least-mean-square fittings can be achieved (especially in regions of moderately low temperatures, where $C_{Vh}(T)$ is of order $C_{Vh}(\infty)/2$) when we use a somewhat more general 9-parameter version of Eq. (A3) containing two additional odd-order ($\propto T^{-5}$ and $\propto T^{-7}$) power terms. Furthermore we can represent (in analogy to Ref. 37) the expansion coefficients, ρ_n, occurring in the denominator of Eq. (A3) by products, $\rho_n \equiv T_s^n r_n(T_s)$ (n =2 and 4 to 8), of n^{th}-order scaling temperature power terms, T_s^n, with corresponding (dimensionless) expansion coefficients, $r_n(T_s)$. An appropriate choice for such scaling temperatures, T_s, turns out to be generally given by taking them to be just coincident with those characteristic (material-specific) temperature points, T_h, at which the respective $C_p(T)$ curves are reaching just 50% of the classical Dulong-Petit value, i. e.

$$T_s \to T_h, \text{ where } \quad C_p(T_h) \equiv 3n_A R/2. \tag{9}$$

Accordingly, we shall use within the present numerical analyses (in Sec. III) a duly general (9-parameter) $\kappa_P(T)$ expression (derived from (A3)) of the T_h-related form

$$\kappa_P(T) = \frac{1 + \frac{c_5}{c_7 T^2} + \frac{c_3}{c_7 T^4}}{\sqrt[2]{1 + \sum\limits_{3\neq n=2}^{8} r_n(T_h)\left(\frac{T_h}{T}\right)^n + \left(\frac{3n_A R}{c_7 T^7}\right)^2}}. \tag{10}$$

A general complication of the analytical apparatus for numerical analyses of measured (isobaric) heat capacities, $C_p(T)$, is due to the circumstance that the latter are in general higher than the harmonic parts, $C_{Vh}(T)$, of isochoric heat capacities. The respective differences, $C_p(T) - C_{Vh}(T) > 0$, are usually very small at temperatures lower than T_h (9). On the other hand, in regions above T_h, where the magnitudes of $\kappa_P(T)$ tend to be comparable with unity, the isobaric heat capacities $C_p(T)$ are generally found to be markedly higher than $C_{Vh}(T)$ (3) due to cumulative effects of

lattice expansion and lattice anharmonicities.[24,28,47,50–52,57,82,91,92] On the background of sufficiently comprehensive low- and high-temperature $C_p(T)$ data sets available for germanium and silicon[5,47] we have devised[50] an obviously adequate formula for the total difference, $C_p(T) - C_{Vh}(T) > 0$. The corresponding analytical expression is of the form[50]

$$C_p(T) - C_{Vh}(T) = 3n_A R\,(\kappa_P(T))^2\left(A_1 T + A_2 T^2 + ...\right), \tag{11}$$

where the expansion coefficients A_n, $n = 1, 2, \ldots$, are representing the cumulative effect of both non-harmonic heat capacity mechanisms in the high temperature region. Consequently, according to Eq. (11), for $C_p(T) - C_{Vh}(T)$, in combination with Eq. (3), for $C_{Vh}(T)$, the temperature dependences of isobaric lattice heat capacities, $C_p(T)$, from absolute zero up to melting points, are represented by the structurally relatively simple formula[43,50,74,82]

$$C_p(T) = 3n_A R\left[\kappa_P(T) + (\kappa_P(T))^2\left(A_1 T + A_2 T^2 + ...\right)\right]. \tag{12}$$

An important advantage of this analytical apparatus is due to the circumstance that, owing to the representation of the heat capacity shape function, $\kappa_P(T)$ (Eq. (4)), by the non-Debye interpolation formula of algebraic type (Eq. (10)), the subsequent applications of Eq. (12) to numerical fittings of experimental $C_p(T)$ data sets do not involve numerical integration procedures.

III. HEAT CAPACITY DATA SELECTIONS AND FITTINGS FOR CUBIC III-V MATERIALS

The analytical apparatus displayed in the preceding section will be seen in the following to be well suited for performing fine numerical fittings, particularly of the thermo-physical $C_p(T)$ data sets, $0 < T < T_r \equiv 298.15$ K, that are available for a variety of cubic III-V materials (GaP, GaAs, GaSb, InP, InAs, and InSb). In view of the usually relatively small differences (<0.5%) between the adiabatic calorimetry $C_p(T)$ data presented for the individual materials in different papers, it turns out to be possible and useful to perform as a rule simultaneous fittings of several, mutually compatible $C_p(T < T_r)$ data sets. In contrast to this, many ones of the respective thermo-chemical $C_p(T > T_r)$ data sets, that are available from different research papers and/or data reviews, are rather inaccurate. Their experimental uncertainties are typically of order 3%, and they may reach even an order of 10%, in certain cases (see below). Moreover one finds in many cases that the lower sections ($T_r \leq T < T_m/2$) of thermo-chemical data sets are more or less incompatible with the respective thermo-physical data sets. In view of such significant uncertainties it is useful to take into consideration some basic criteria that may be invoked for preliminary assessments of probable compatibility vs. clear incompatibility of different high-temperature data sets, $C_p^{high}(T \geq T_r)$, with their more reliable (well-established) low-temperature counterparts, $C_p^{low}(T \leq T_r)$.

A. Basic criteria for high-temperature data selections

Consider first the immediate vicinity of the commonly considered reference point, $T_r = 298.15$ K, where the low- and high-temperature $C_p(T)$ data points should naturally tend to the same magnitude,[17]

$$C_p^{high}(T \to T_r) = C_p^{low}(T \to T_r). \tag{13}$$

In addition to this, in order to assure a smooth match of the respective data sets in the room temperature region, one has still to require analogous coincidences also with respect to their low-order derivatives,

$$\frac{d^n C_p^{high}(T \to T_r)}{(dT)^n} = \frac{d^n C_p^{low}(T \to T_r)}{(dT)^n}, \quad n = 1, 2, \ldots, \tag{14}$$

(i. e., above all, for their slopes,[17] $n = 1$, and curvatures, $n = 2$). Unfortunately, as we will see below, these basic requirements are only seldom fulfilled. The frequent deficiencies in this respect are obvious in particular for those high-temperature data sets which are given in form of various linear "approximations", $C_p^{high(lin.)}(T) \approx a + bT$ (for numerous examples of such raw data sets see in particular the thermo-chemical data reviews).[4–6] It is frequently found that low-temperature data sets show a pronounced non-vanishing curvature (convex shape) in the vicinity of the reference point,

$d^2C_p^{low}(T)/(dT)^2 < 0$ ($T \approx T_r$), whereas such linear high-temperature data sets show no curvature at all, $d^2C_p^{high(lin.)}(T)/(dT)^2 = 0$. An actually satisfactory match between such $C_p^{high(lin.)}(T)$ and $C_p^{low}(T)$ data sets in the room temperature region can thus generally not be achieved. On the other hand, even in view of such notorious misfits in the vicinity of T_r, it can not a priori be excluded that at least some upper sections of such $C_p^{high(lin.)}(T)$ data sets (e. g. for $T > 400$ K) are acceptable as reasonable continuations of $C_p^{low}(T)$ data sets in the high temperature region.

With respect to the latter eventuality it is important to consider still another basic criterion for distinguishing cases of possible admissibility vs. clear inadmissibility of a various $C_p^{high}(T > T_r)$ data sets. To this end we note that the differences $C_p(T) - C_{Vh}(T) > 0$ (11) use to be monotonically increasing functions everywhere (from 0 up to melting points), i. e.

$$d(C_p(T) - C_{Vh}(T))/dT > 0, \tag{15}$$

(see also Sec. V). This monotonic behavior of the anharmonicity-related differences implies, among other things, that their magnitudes in the high-temperature region must throughout be larger than at the reference point,

$$0 < C_p^{low}(T_r) - C_{Vh}(T_r) < C_p^{high}(T > T_r) - C_{Vh}(T > T_r). \tag{16}$$

A possible conflict of a given $C_p^{high}(T)$ data set with this basic property (16) can be easily verified provided that the harmonic part, $C_{Vh}(T) \propto \kappa_P(T)$ (3), is already known (for any T) from a preliminary fitting of an associated thermo-physical data sets, $C_p^{low}(T)$ (on the basis of Eq. (12), in combination with (10)).

On the background of the preceding criteria, let us briefly comment on the collections of data sets that can actually be involved into - or a priori excluded from - the fitting processes for the individual materials under study.

B. Fittings of compatible low- and high-temperature data sets

For the case of GaP (see Fig. 1), detailed experimental information on the heat capacity at very low temperatures (2 K to 37 K) was available from the study by Abrahams and Hsu[54] in terms of the corresponding Debye temperatures, $\Theta_D(T)$ (cf. Fig. 1 in Ref. 54). We have retransformed the latter in the usual way (cf. Sec. IV) into a corresponding cryogenic $C_p(T)$ data set (○). The continuation towards room temperature was given by two sets of smoothed $C_p^{low}(T)$ data (up to 300 K) from Refs. 57 (△) and 91 (□). Furthermore we have included into the fitting process the apparently representative sets of smoothed (nearly coinciding) $C_p^{high}(T)$ values given in Refs. 5 (☆), 6 (∗) and 9 (◀). From the simultaneous least-mean-square fitting of these six partial $C_p(T)$ data sets (up to 1700 K) we have obtained the parameter values listed in Table I.

Qualitatively more or less different sets of $C_p^{high}(T)$ data are available for the range 800 K to 1500 K from Ref. 10 (◇) and for the range 370 K to 730 K from Ref. 15 (×). At first sight, the latter $C_p^{high}(T)$ data sets appear to be compatible, too, with the $C_p^{low}(T)$ data considered above. A corresponding alternative fit leads to similar values of parameters (occurring in Eq. (10)), whereas the value for A_1, which follows from such an alternative fit (via Eq. (12)), turns out to be by a factor of about 3 lower than the preceding one (cf. Table I). Yet, notwithstanding the similarly good quality of the latter fit in comparison with the preceding one, there are some physical reasons for rejecting it as an obviously less adequate picture of the high-temperature behavior. (See the corresponding argumentation in Sec. IV C.)

Clearly incompatible with the low-temperature behavior is the $C_p^{high(lin.)}(T)$ data set given in Ref. 4 (■) (cf. Fig. 1). These data are not only in strong conflict with the continuity equation (14) for the first- and second-order derivatives, but even with the basic requirement (16). Actually, we see from Fig. 1 that the respective $C_p^{high(lin.)}(T)$ data points (■), from T_r up to 1100 K, are located below the extrapolated $C_{Vh}(T)$ curve, $C_p^{high(lin.)}(T) < C_{Vh}(T)$. Furthermore we see from Fig. 1 that, in view of an actual difference of $C_p^{low}(T_r) - C_{Vh}(T_r) = 0.61$ J/(mol · K) at the reference point, the $C_p^{high(lin.)}(T)$ data set due to Ref. 4 (■) is in conflict with the basic requirement (16) even up to

TABLE I. Adjusted coefficients $r_2(T_h)$ to $r_8(T_h)$ and c_3 to c_7 due to Eq. (10) for the harmonic lattice heat capacity shape function, $\kappa_P(T)$, and associated anharmonicity-related coefficients, A_1 and A_2, due to Eq. (12). For the commonly considered thermo-chemical reference temperature, $T_r = 298.15$ K, we have quoted the corresponding isobaric heat capacities, $C_p(T_r)$ (12), entropies, $S_p(T_r)$ (17), and enthalpy differences, $\Delta H_p(T_r) \equiv H_p(T_r) - H_p(0)$ (17).

	GaP	GaAs	GaSb	InP	InAs	InSb
T-ranges (K)	1 to 1750	1 to 1500	1 to 950	1 to 900	1 to 1200	1 to 750
A_2 (K^{-2})	2.850×10^{-9}	7.170×10^{-8}	1.313×10^{-7}	–	1.162×10^{-7}	1.497×10^{-7}
A_1 (K^{-1})	4.927×10^{-5}	3.133×10^{-5}	4.813×10^{-5}	4.496×10^{-5}	4.660×10^{-5}	5.751×10^{-5}
$T_s^{(fixed)} = T_h$ (K)	**115.5**	**86.0**	**68.7**	**93.4**	**69.3**	**55.5**
$r_2(T_h)$	1.786	1.744	1.727	2.298	2.120	1.940
$r_4(T_h)$	3.013	2.349	2.764	2.672	1.928	2.401
$r_5(T_h)$	−2.612	−1.556	−2.113	−2.782	−1.443	−1.865
$r_6(T_h)$	1.112	0.595	0.768	1.172	0.491	0.634
$r_7(T_h)$	−0.2156	−0.1123	−0.1284	−0.2170	−0.0748	−0.0967
$r_8(T_h)$	0.01930	0.01242	0.01040	0.01628	0.00547	0.00652
c_7 ($JK^{-8}mol^{-1}$)	6.681×10^{-10}	5.947×10^{-9}	4.968×10^{-8}	8.474×10^{-9}	7.428×10^{-8}	4.496×10^{-7}
c_5 ($JK^{-6}mol^{-1}$)	8.044×10^{-8}	5.466×10^{-8}	2.199×10^{-7}	1.326×10^{-6}	3.376×10^{-7}	–
c_3 ($JK^{-4}mol^{-1}$)	4.545×10^{-5}	9.566×10^{-5}	2.051×10^{-4}	1.241×10^{-4}	2.547×10^{-4}	4.613×10^{-3}
$C_p(T_r)$ (J/(mol · K))	44.10	47.03	48.79	45.35	48.24	49.65
$S_p(T_r)$ (J/(mol · K))	51.38	64.15	75.79	63.27	75.68	86.85
$\Delta H_p(T_r)$ (J/mol)	8047	9463	10465	9005	10317	11212

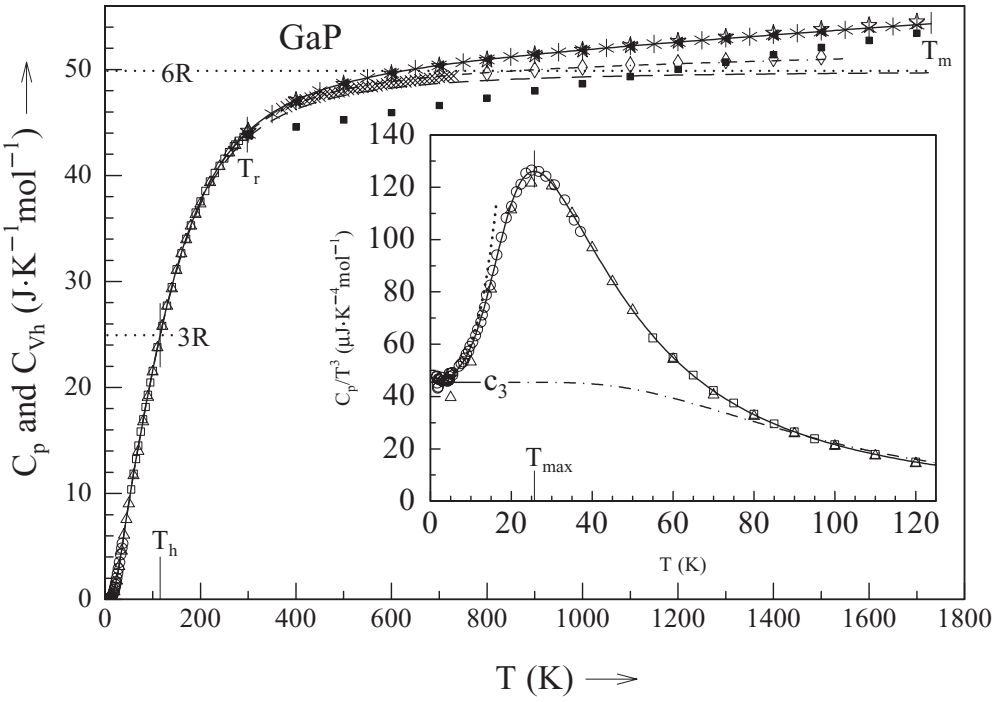

FIG. 1. Fitting of the $C_p^{low}(T)$ data sets available for GaP from Ref. 54 (○), 57 (△), and 91 (□), and in combination with the $C_p^{high}(T)$ data sets due to Refs. 5 (☆), and 6 (∗), and 9 (◀). Shown for comparison are also the more or less strongly deviating $C_p^{high}(T)$ data sets given in Ref. 4 (■), 10 (◊), and 15 (×). $C_p(T)$ and $C_p(T)/T^3$ curves (———, Eq. (12)); $C_{Vh}(T) \propto \kappa_P(T)$ curves (– – – –, Eqs. (3) and (10)); asymptotic $C_{Vh}(T)/T^3 \to 0$ curve (· · · · · · · · · , Eq. (8)); Debye's $C_D(T)/T^3$ curve for $\Theta_D = \Theta_D(0)$, as quoted in Table III (· - · - · - · , Eq. (2)). (Note that the same associations between different curve types and the underlying analytical expressions apply also to the subsequent Figs. 2 to 6). The deviating high-temperature $C_p(T)$ curve (– – · – – · – –, Eq. (12)) corresponds to data given in Ref. 10 (◊) and 15 (×).

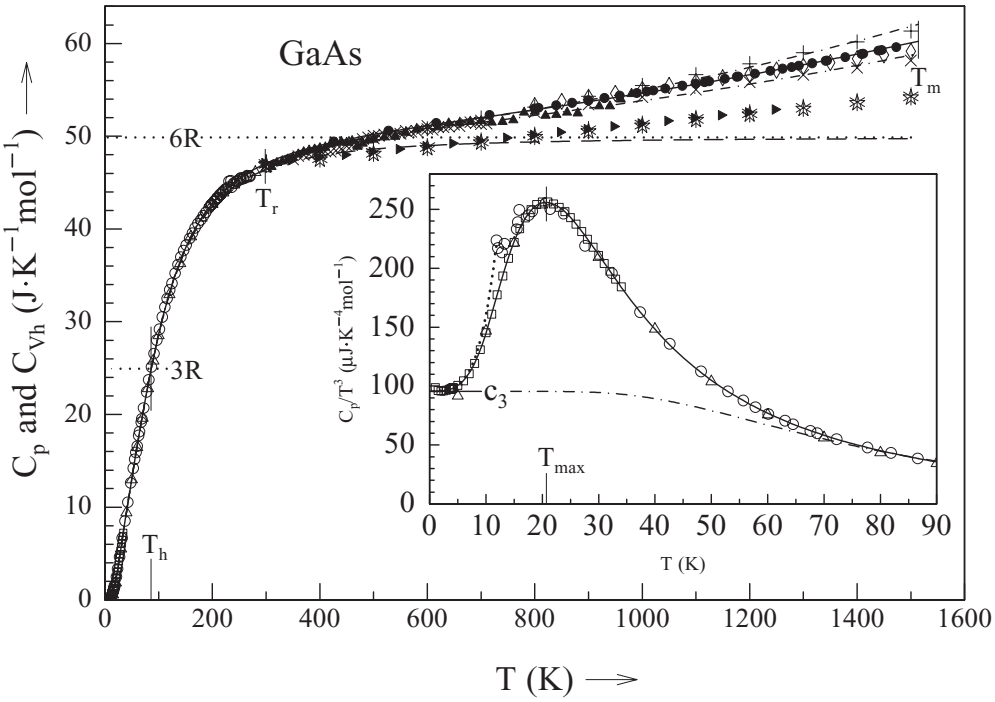

FIG. 2. Fitting of the $C_p^{low}(T)$ data sets available for GaAs from Ref. 32 (□), 52 (○), and 58 (△) in combination with the novel $C_p^{high}(T)$ data set (●) resulting from the present re-assessment (cf. Sec. IV) of original enthalpy data due to Refs. 10 and 20. Shown for comparison are also the more or less strongly deviating $C_p^{high}(T)$ data sets given in Refs. 5 (☆), 6 (∗), 10 (♢), 12 (×), 19 (►), 20 (+), and 93 (▲). Possible alternative fits of the same $C_p^{low}(T)$ data sets in combination with $C_p^{high}(T)$ data due to Ref. 12 (×) and 20 (+) are indicated by double-dashed-dotted curves.

1200 K. Consequently, from physical points of view, the latter data set can be looked upon as a quite erroneous one.

For GaAs, GaSb, InAs, and InSb, rather detailed and highly informative cryogenic $C_p(T)$ data sets are available in tabulated form from Ref. 32 (□). Further low-temperature data (up to 273.2 K) had been given for these materials (including InP) in form of tables of smoothed $C_p^{low}(T)$ values by Piesbergen.[51] Yet, in order to draw maximum possible pieces of information from the original $C_p(T)$ measurements performed by Piesbergen,[51] we have re-digitized the individual (unsmoothed) Debye temperature values, $\Theta_D(T)$, which had been presented in graphical form in Refs. 51 and 52. The respective (transformed) $C_p^{low}(T)$ data points (○) are shown in the following figures.

Consider now in more detail the case of GaAs (Fig. 2). For the low-temperature region we have used, above all, the above mentioned $C_p^{low}(T)$ data sets available from Refs. 32 (□) and 52 (○). Furthermore we have included into the fitting process a smoothed $C_p^{low}(T)$ data set given in Ref. 58 (△). Among the large variety of different $C_p^{high}(T)$ data sets shown in Fig. 2, several ones turned out to be at least roughly compatible with the three $C_p^{low}(T)$ data sets in consideration. This concerns the $C_p^{high(lin.)}(T)$ data given in Ref. 20 (+) and the estimated $C_p^{high}(T)$ data quoted in Table 5 of Ref. 12 (×). The corresponding approximate fits are represented by the upper and lower double-dashed-dotted curves, respectively, in Fig. 2. We see, among other things, that the majority of the $C_p^{high}(T)$ data points given for the range 800 K to 1500 K in Ref. 10 (♢) are ranging within the middle region between these two alternative curves, and that the residual uncertainty increases, with increasing T, up to an order of 3 J/(Kmol) (in the vicinity of T_m). In order to reduce this uncertainty we have re-evaluated some genuine experimental data for enthalpy differences, $\Delta H_p(T) \equiv H_p(T) - H_p(T_r)$, that are available in graphical form from Refs. 10 and 20. (For a brief sketch of the corresponding analysis see Sec. IV). We have derived from these enthalpy data a novel (clearly non-linear) sequence of $C_p^{high}(T)$ data points (●). Fitting, finally, the latter $C_p^{high}(T)$ data in

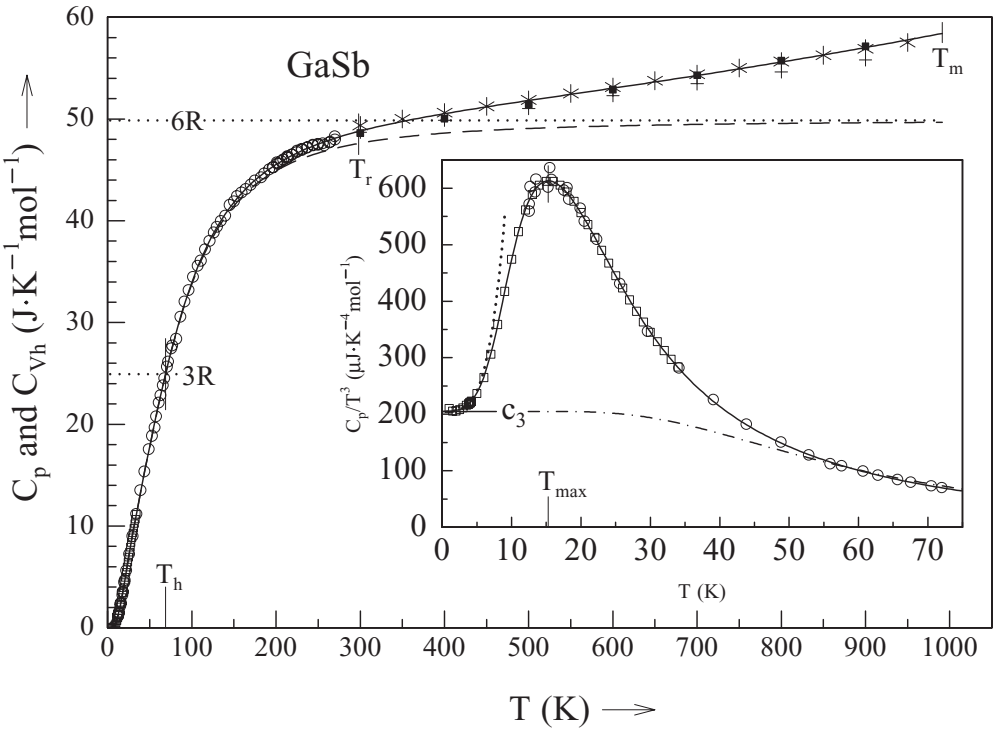

FIG. 3. Fitting of the $C_p^{low}(T)$ data sets available for GaSb from Ref. 32 (□) and 52 (○), in combination with the $C_p^{high}(T)$ data sets due to Ref. 4 (■), and 6 (∗). Shown for comparison is also the slightly deviating $C_p^{high}(T)$ data set due to Ref. 21 (+).

combination with the three aforementioned $C_p^{low}(T)$ data sets we have obtained the respective set of parameter values given in Table I.

Let us still assess, in the light of the present fit (solid curve in Fig. 2), some other $C_p^{high}(T)$ data sets which were obtained via direct heat capacity measurements by the differential scanning calorimetry (DSC) technique. Viewing the unsmoothed $C_p^{DSC}(T)$ data given for the range of 310 K to 980 K in Ref. 93 (▲) we find a relatively good agreement in the vicinity of 400 K, whereas the deviations from the fitted (solid) curve reach on order of 2%, in the vicinity of 800 K. Comparable deviations (up to an order of 3%) are also shown by the $C_p^{DSC}(T)$ data given for the range of 350 K to 710 K in Table IV of Ref. 12 (×).

Clearly incompatible with the low-temperature behavior are the $C_p^{high(lin.)}(T)$ data points given for GaAs in Ref. 19 (►) and in two thermo-chemical data reviews (Refs. 5 (☆) and 6 (∗)). These data sets are not only in clear conflict with the continuity equation (14), for the first- and second-order derivatives, but even with the basic requirement (16). We see immediately from Fig. 2 that several ones of these data points are located even below the extrapolated $C_{Vh}(T)$ curve, $C_p^{high(lin.)}(T) < C_{Vh}(T)$. This is the case for $C_p^{high(lin.)}(T)$ values due to Ref. 6 (∗) and 19 (►) (up to 600 K), and Ref. 5 (☆) (up to 680 K). Furthermore we see from Fig. 2 that, in view of an estimated difference of $C_p^{low}(T_r) - C_{Vh}(T_r) = 0.72$ J/(mol · K) at the reference point, the $C_p^{high(lin.)}(T)$ data sets due to Refs. 5 (☆), 6 (∗), and 19 (►) are in conflict with the requirement (16) even up to about 800 K. Consequently, from basic physical points of view, these three $C_p^{high(lin.)}(T)$ data sets can be looked upon as largely inadequate (erroneous) ones.

For the case of GaSb (Fig. 3), the low-temperature region was well-represented, again, by the aforementioned $C_p^{low}(T)$ data sets available from Refs. 32 (□) and 52 (○). Furthermore we have included into the fitting process two $C_p^{high(lin.)}(T)$ data sets given in Refs. 4 (■) and 6 (∗), which turned out to be (at least roughly) compatible with the low-temperature data in consideration. From the simultaneous least-mean-square fitting of these four partial $C_p(T)$ data sets (up to 950 K) we

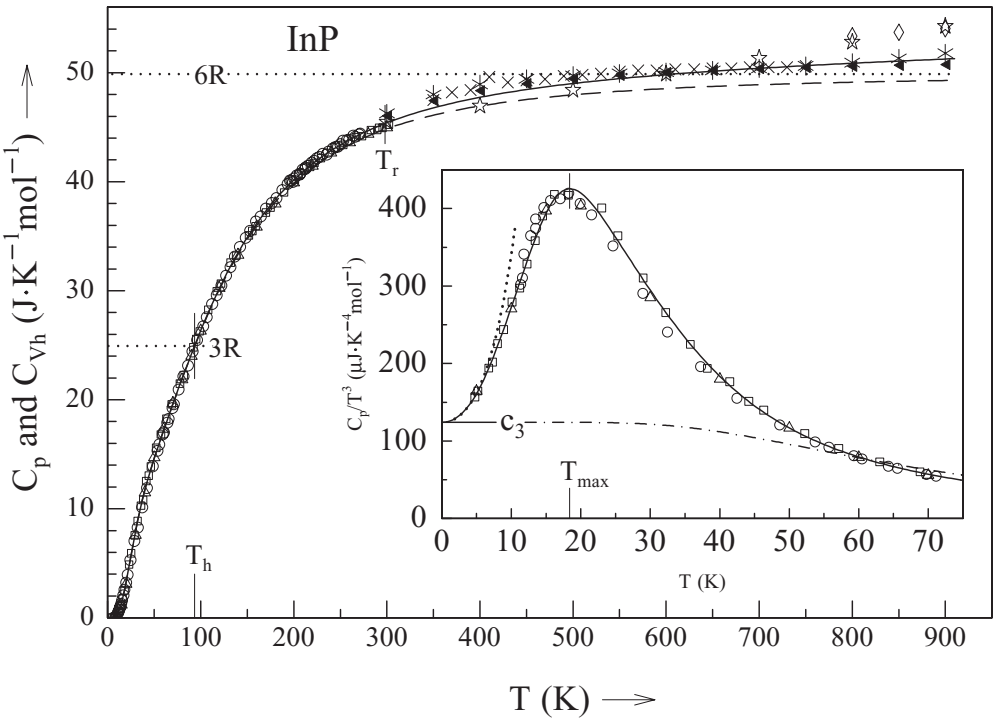

FIG. 4. Fitting of the low-temperature $C_p(T)$ data sets available for InP from Refs. 52 (○), 60 (△), and 94 (□) in combination with the $C_p^{high}(T)$ data set due to Ref. 9 (◀) and partial sections (see the text) of the $C_p^{high}(T)$ data sets due to Refs. 5 (☆), 6 (∗), and 16 (×). Shown for comparison are also the markedly deviating $C_p^{high}(T)$ data points quoted in Ref. 5 (☆) and 10 (◊) for the region 800 K $\leq T \leq$ 900 K (i. e. close to the phase transition point).

have obtained the parameter values listed in Table I. The alternative $C_p^{high(lin.)}(T)$ data set given in Ref. 21 (+) has not been taken into consideration in view of a markedly weaker slope, which leads to a deviation of about 3 J/(Kmol) (corresponding to about 4%) in the vicinity of T_m. This residual uncertainty might serve as a challenge for forthcoming heat capacity (or enthalpy) measurements in this region.

For the case of InP (Fig. 4), in view of the relative scarcity of data available for the liquid-helium-hydrogen region, we have considered here the $C_p^{low}(T)$ data resulting from the aforementioned re-digitations of the individual $\Theta_D(T)$ points shown in Ref. 52 (○) and the somewhat more extended data sets (5 K $< T <$ 300 K) due to Ref. 60 (△) and 94 (□) in combination with the $C_p^{high}(T)$ data set due to Ref. 9 (◀), the lower section ($T <$ 700 K) of the $C_p^{high}(T)$ data set due to Ref. 5 (☆), and the upper sections ($T >$ 600 K) of the $C_p^{high}(T)$ data due to Ref. 6 (∗) and 16 (×). From the simultaneous least-mean-square fitting of these seven partial $C_p(T)$ data sets (up to 900 K) we have obtained the parameter values listed in Table I. (Note that the upper end of the calculated $C_p(T)$ curve, at 910 K, corresponds to the first phase transition point for InP.) We see also from Fig. 4 that the upper section ($T >$ 700 K) of the $C_p^{high(lin.)}(T)$ data set due to Ref. 5 (☆), similarly as the few $C_p^{high}(T)$ data points due to Ref. 10 (◊), deviate significantly from the common trend in the respective region (i. e. from 800 K up to the phase transition point).

For the case of InAs (Fig. 5), the low-temperature region is well represented by the $C_p^{low}(T)$ data sets available from Refs. 32 (□), 52 (○), and 60 (△). In contrast to this, we are concerned in the high-temperature region with very large discrepancies between different $C_p^{high}(T)$ data sets. These discrepancies are seen from Fig. 5 to increase up to an unusually large magnitude of about 14%, in the vicinity of the melting point. Consider first the group of lower $C_p^{high(lin.)}(T)$ data points, which is characterized by $C_p(T_m)$ values of about 56 J/(mol · K) (due to Ref. 4 (■)) or about 55 J/(mol · K) (due to Refs. 5 (☆), 6 (∗), and 19 (►)). From this group of lower $C_p^{high(lin.)}(T)$ data

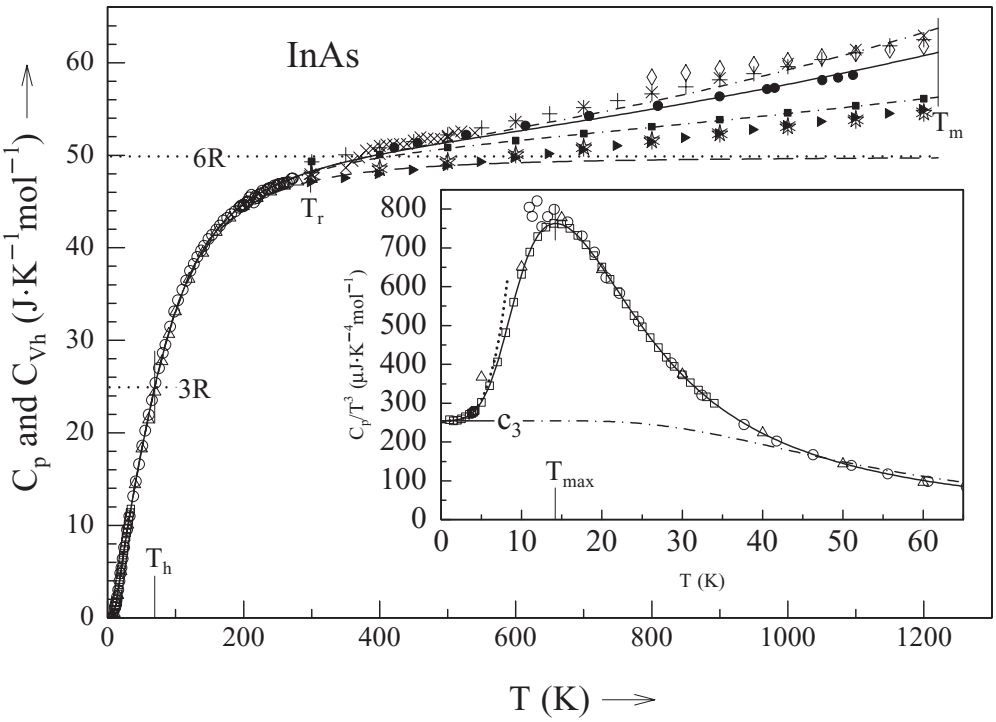

FIG. 5. Fitting of the $C_p^{low}(T)$ data sets available for InAs from Ref. 32 (□), 52 (○), and 60 (△) in combination with the novel $C_p^{high}(T)$ data set (●) resulting from the present re-assessment of original enthalpy data due to Ref. 20 (cf. Sec. IV). Shown for comparison are also the more or less strongly deviating $C_p^{high}(T)$ data sets given in Refs. 4 (■), 5 (☆), 6 (∗), 10 (◊), 13 (×), 19 (►), and 20 (+). Possible alternative fits of the same constellation of $C_p^{low}(T)$ data sets in combination with the upper section (800 K $< T <$ 1200 K) of the $C_p^{high}(T)$ data set due to Ref. 20 (+) or with the upper section (400 K $< T <$ 1200 K) of the $C_p^{high}(T)$ data set due to Ref. 4 (■) are represented by double-dashed-dotted curves.

points, the only one, which we have found to be largely compatible (for $T > 400$ K, at least) with the aforementioned $C_p^{low}(T)$ data sets, is that one due to Ref. 4 (■). The corresponding (tentative) fit is indicated by the lower double-dashed-dotted curve. Clearly incompatible with the low-temperature behavior are the $C_p^{high(lin.)}(T)$ data points given in Refs. 5 (☆), 6 (∗), and 19 (►). Apart from the obvious conflict of these three sequences of $C_p^{high(lin.)}(T)$ data points with the continuity equation (14) for the first- and second-order derivatives, these data sets are, in view of an estimated difference of $C_p^{low}(T_r) - C_{Vh}(T_r) = 0.81$ J/(mol · K) at the reference point, in disagreement again with the basic requirement (16) (from T_r up to an order of 600 K). Consequently, from basic physical points of view, these three $C_p^{high(lin.)}(T)$ data sets can by no means be considered as possible continuations of the given $C_p^{low}(T)$ data sets into the high-temperature region.

Consider now the group of higher $C_p^{high}(T)$ data points due to Refs. 10 (◊) and 20 (+), which are tending to an order[13] of $C_p(T_m) \approx 63$ J/(mol · K) near the melting point. (Note that such a $C_p(T_m)$ value[13] is obviously the highest one among the counterparts reported in literature for the six III-V materials under study). We have found that the limited set ($T \geq 800$ K) of $C_p^{high}(T)$ data points due to Ref. 10 (◊) is largely incompatible with the $C_p^{low}(T)$ data sets in consideration. In contrast to this, it was possible to include at least the upper section ($T \geq 800$ K) of the $C_p^{high(lin.)}(T)$ data set due to Ref. 20 (+) into an alternative fitting process without causing a significant deterioration of a separate, excellent fit of the three $C_p^{low}(T)$ data sets. The respective $C_p(T)$ dependence is represented by the upper double-dash-dotted curve in Fig. 5. A peculiar feature of the latter curve is the qualitative change of its curvature from convex shape (in the vicinity of T_r) to a pronounced concave shape (from about 600 K up to T_m). This snake-like behavior of the upper double-dashed-dotted curve is in contrast to former fittings[13,17] where, owing to the use of the oversimplified Maier-Kelley

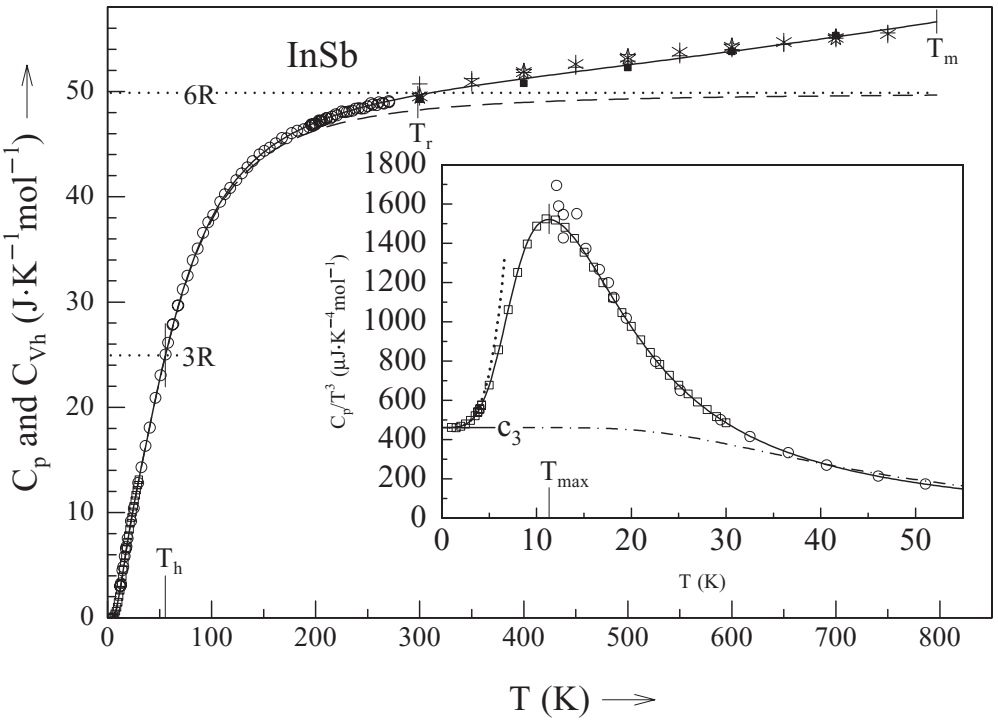

FIG. 6. Fitting of the $C_p^{low}(T)$ data sets available for InSb from Ref. 32 (□) and 52 (○) in combination with the non-linear $C_p^{high}(T)$ data sets due to Refs. 5 (☆) and 6 (∗) and the $C_p^{high(lin)}(T)$ data set due to Ref. 4 (■). Shown for comparison is also the $C_p^{high(lin)}(T)$ data set due to Ref. 21 (+).

equation (1), the corresponding $C_p(T)$ curves retained automatically a weak convex (nearly linear) shape through the whole high-temperature region.

In view of the unusually large divergence (of order 6 J/(mol · K)) between the magnitudes of fictitious $C_p(T_m)$ values estimated via the two preceding alternative fittings, we have re-evaluated (in analogy to the case of GaAs) the genuine experimental data for enthalpy differences, $\Delta H_p(T) \equiv H_p(T) - H_p(T_r)$, that are available in graphical form from Ref. 20 (cf. Sec. IV). In this way we have derived a novel set of $C_p^{high}(T)$ data points (●). (Observe the approximate equality of the latter with the unsmoothed $C_p^{DSC}(T)$ data points quoted for the range of 350 K to 540 K in Table IV of Ref. 13 (×)). Fitting these re-evaluated $C_p^{high}(T)$ data points (●) in combination with the three aforementioned $C_p^{low}(T)$ data sets we have obtained the respective set of parameter values quoted for InAs in Table I.

Finally, for the case of InSb (Fig. 6), the low-temperature region was well represented, again, by the $C_p^{low}(T)$ data sets available from Refs. 32 (□) and 52 (○). Furthermore we have included into the fitting process the non-linear $C_p^{high}(T)$ data sets due to Refs. 5 (☆) and 6 (∗) and the $C_p^{high(lin)}(T)$ data set due to Ref. 4 (■). From the simultaneous least-mean-square fitting of these five partial $C_p(T)$ data sets (up to 750 K) we have obtained the parameter values listed in Table I. Shown in Fig. 6 is also the $C_p^{high(lin)}(T)$ data set due to Ref. 21 (+), the lower section of which ($T < 400$ K) is in clear disagreement with the continuity conditions (13) and (14).

Henceforth, on the basis of the material-specific parameter sets listed in Table I, it is in principle possible to pre-calculate, by means of numerical integrations, the magnitudes of thermodynamic standard functions like entropies and enthalpies,

$$S_p(T) = \int_0^T dT' C_p(T')/T' \quad and \quad H_p(T) - H_p(0) = \int_0^T dT' C_p(T'), \tag{17}$$

for any T, from absolute zero up to the individual melting points, T_m (or the first phase transition point, in the case of InP). For brevity we have quoted in Table I, at least, the magnitudes of these two quantities, $S_p(T_r)$ and $\Delta H_p(T_r) \equiv H_p(T_r) - H_p(0)$, for $T_r = 298.15$ K, which are of the utmost interest within thermo-chemistry (see also Sec IV). Furthermore, for the sake of detailed numerical comparisons of presently estimated (smoothed) $C_p(T)$ values with their more or less different predecessors, that have been given in tabulated form for low- and/or high temperatures in former research papers[12–16,32,51,58–60,93] and in data reviews,[2–6] we give in Table II representative sets of discrete (smoothed) $C_p(T)$ values resulting from Eq. (12) (in combination with Eq. (10)) on the basis of the parameter values quoted in Table I.

IV. DETERMINATION AND ASSESSMENT OF VARIABLE DEBYE TEMPERATURES

Within the frame of the original Debye model,[23–27,65] the generally very complicated ε-dependences of material-specific spectral functions, $g_P(\varepsilon)$, in Eq. (4), had been approximated simply by a quadratic parabola, $\varepsilon_D(0 \le \varepsilon \le \varepsilon_D) \propto \varepsilon^2$, where $\varepsilon_D \equiv k_B\Theta_D$ represents a fictitious cut-off energy and Θ_D denotes the respective Debye temperature. According to this (grossly oversimplified) model, the temperature dependences of isochoric heat capacity $C_{Vh}(T)$ (3), follow readily from Eq. (4) to adapt the very special (fictitious) form[23–27,52,65,90]

$$C_D(T) \equiv 3n_A R\kappa_D(T) = 9n_A R\left(\frac{T}{\Theta_D}\right)^3 \int_0^{\Theta_D/T} dx \frac{x^4 e^x}{(e^x-1)^2}. \tag{18}$$

However, numerous analyses of heat capacity data sets, which were available already for years for a large variety of group-IV, III-V, and II-VI materials (cf. Ref. 74 and papers there cited), alkali halides,[28,29] as well as various classes of ternary materials (e. g. chalcopyrites[81] or perovskite-type oxides),[95] have continually shown that the original Debye model expression (18) for heat capacities is throughout incapable (for fixed Θ_D) of providing reasonable numerical simulations of measured temperature dependences. This general statement applies in particular to the cryogenic region. Actually, we see from the insets to Figs. 1 to 6 that the empirical behavior of the relevant ratios,[33–44]

$$C_p(T)/T^3 \equiv \rho(T), \tag{19}$$

are showing throughout rather pronounced non-monotonic (local maximum) behaviors.

In contrast to these empirical findings, the theoretical counterpart of Debye type, $C_D(T)/T^3 \equiv \rho_D(T)$ (cf. Eq. (2)), shows a priori a fictitious $T \to 0$ plateau behavior,[37] $\rho_D(T \to 0) \cong c_3$ (from 0 up to temperatures of about $\Theta_D/12$), which is followed by an exclusively monotonic decrease,[37] $d\rho_D(T)/dT < 0$, for any $T > \Theta_D/12$ (see the dashed-dotted curves in the insets to Figs. 1 to 6).

A. Analytical descriptions and calculations of variable Debye temperatures

A frequently chosen way for dealing with this general breakdown of Debye's original model consisted for a long time in continual invocations of the largely artificial concept of effective (T-dependent) Debye temperatures,[2,3,23–29,31,32,45–62,65,88] $\Theta_D(T)$. These quantities are well known to be defined, implicitly, by an integral representation of the form[24–27,45,50,52]

$$C_p(T) = 9n_A R\left(\frac{T}{\Theta_D(T)}\right)^3 \int_0^{\Theta_D(T)/T} dx \frac{x^4 e^x}{(e^x-1)^2}. \tag{20}$$

(Note that, for the materials under study, some fragmentary sections of such $\Theta_D(T)$ curves had already been shown in Refs. 51 to 62.)

On the basis of equation (20) one can perform point-by-point transformations of individual isobaric heat capacity values, $C_p(T)$, into the respective Debye temperature values, $\Theta_D(T)$. Corresponding representative results are shown for GaP, GaAs, and GaSb in Fig. 7 and for InP, InAs, and InSb in Fig. 8. From these figures we see, among other things, that the cryogenic sections of the $\Theta_D(T)$

TABLE II. Collection of smoothed isobaric heat capacity values, C_p (J/(mol · K)), due to Eq. (12) (in combination with Eq. (10)), and the corresponding effective Debye temperatures, Θ_D (K), due to Eq. (20).

	GaP		GaAs		GaSb		InP		InAs		InSb	
T (K)	C_p	Θ_D	C_p	Θ_D	C_p	Θ_D	C_p	Θ_D	C_p	Θ_D	C_p	Θ_D
0	0.0	440.6	0.0	343.8	0.0	266.6	0.0	315.3	0.0	248.1	0.0	203.5
2	0.000366	439.5	0.000768	343.4	0.001654	265.9	0.001036	310.8	0.002057	247.3	0.003744	202.5
4	0.00300	436.0	0.00627	341.1	0.01409	260.4	0.00941	297.9	0.01775	241.1	0.03572	191.0
6	0.01062	429.3	0.02260	333.7	0.05747	244.5	0.03852	279.3	0.07474	224.0	0.18428	165.8
8	0.02713	418.6	0.06121	319.2	0.18344	221.4	0.1136	259.7	0.2458	200.8	0.6429	145.7
10	0.05895	404.0	0.14484	299.4	0.47319	201.8	0.2725	242.5	0.6323	183.2	1.4875	137.7
12	0.11642	386.4	0.3064	279.9	0.9723	190.4	0.5614	228.7	1.2629	174.5	2.6150	136.5
14	0.2145	367.7	0.5741	264.9	1.6636	185.6	1.0251	218.3	2.0928	171.8	3.9095	138.4
16	0.3708	350.2	0.9580	255.2	2.5047	184.7	1.6776	211.5	3.0664	172.2	5.2563	142.0
18	0.6002	335.5	1.4531	249.7	3.4483	186.0	2.4782	208.5	4.1235	174.5	6.565	146.8
20	0.9085	324.7	2.0443	247.3	4.4474	188.7	3.3599	208.5	5.2044	178.2	7.796	152.3
25	1.9684	313.2	3.8005	249.6	6.598	199.3	5.672	215.6	7.773	190.6	10.572	167.1
30	3.2820	315.4	5.710	258.1	9.320	212.0	7.955	226.6	10.068	204.9	13.123	180.9
35	4.721	323.2	7.616	269.1	11.545	224.5	10.003	239.7	12.191	218.8	15.589	192.8
40	6.207	333.4	9.484	280.5	13.691	236.0	11.742	254.6	14.224	231.4	18.000	202.7
45	7.585	344.6	11.318	291.4	15.787	246.1	13.244	270.1	16.201	242.5	20.341	210.8
50	9.128	356.4	13.123	301.4	17.836	254.7	14.606	285.3	18.127	252.2	22.589	217.4
55	10.522	368.3	14.899	310.5	19.832	262.0	15.894	299.7	19.994	260.6	24.722	222.8
60	11.872	379.9	16.642	318.5	21.763	268.1	17.144	313.0	21.794	267.8	26.726	227.1
65	13.183	391.0	18.346	325.5	23.617	273.2	18.372	325.2	23.519	274.0	28.592	230.6
70	14.463	401.5	20.004	331.6	25.385	277.3	19.581	336.3	25.161	279.4	30.317	233.3
75	15.716	411.2	21.609	336.9	27.058	280.7	20.773	346.3	26.716	284.0	31.903	235.5
80	16.945	420.2	23.154	341.4	28.634	283.4	21.944	355.3	28.183	287.9	33.354	237.2
85	18.149	428.5	24.635	345.3	30.109	285.5	23.092	363.5	29.560	291.3	34.679	238.5
90	19.329	436.0	26.050	348.6	31.485	287.2	24.212	370.8	30.849	294.1	35.885	239.4
95	20.485	442.9	27.395	351.4	32.764	288.4	25.301	377.4	32.053	296.6	36.983	240.1
100	21.613	449.1	28.669	353.7	33.950	289.3	26.357	383.3	33.175	298.6	37.981	240.5
110	23.786	459.7	31.010	357.3	36.060	290.3	28.363	393.4	35.191	301.8	39.716	240.8
120	25.836	468.2	33.083	359.7	37.860	290.4	30.218	401.4	36.932	304.0	41.156	240.3
130	27.755	474.9	34.907	361.2	39.392	289.8	31.921	407.9	38.436	305.4	42.359	239.3
140	29.539	480.1	36.509	361.9	40.700	288.7	33.474	413.1	39.736	306.1	43.370	237.8
150	31.187	484.0	37.912	362.1	41.818	287.2	34.885	417.1	40.864	206.2	44.228	235.8
160	32.703	486.9	30.142	361.8	42.781	285.2	36.162	420.3	41.845	305.7	44.961	233.3
170	34.093	488.9	40.223	361.1	43.612	282.8	37.318	422.7	42.704	304.8	45.594	230.3
180	35.362	490.2	41.173	360.1	44.336	280.0	38.362	424.5	43.458	303.5	46.144	226.7
190	36.520	490.9	42.012	358.8	44.969	276.8	39.306	425.7	44.125	301.6	46.626	222.5
200	37.575	491.0	42.755	357.2	45.527	273.1	40.159	426.4	44.716	299.4	47.053	217.6
210	38.537	490.7	43.415	355.3	46.022	269.0	40.931	426.8	45.244	296.6	47.434	212.0
220	39.412	490.0	44.005	353.2	46.463	264.3	41.630	426.7	45.781	293.4	47.777	205.5
230	40.210	488.9	44.533	360.8	46.860	259.0	42.266	426.3	46.146	289.6	48.087	197.9
240	40.938	487.5	45.008	348.1	47.218	253.1	42.843	425.6	46.533	285.2	48.370	189.2
250	41.603	485.9	45.438	345.1	47.544	246.4	43.370	424.7	46.887	280.3	48.630	179.1
260	42.211	483.9	45.827	341.8	47.842	238.9	43.850	423.4	47.211	274.6	48.870	167.2
270	42.768	481.7	46.182	338.2	48.167	230.4	44.291	421.8	47.509	268.2	49.094	153.1
280	43.279	479.3	46.506	334.2	48.371	220.7	44.695	420.0	47.784	261.0	49.303	135.9
290	43.748	476.6	46.804	329.8	48.607	209.6	45.066	418.0	48.040	252.9	49.500	(114)
300	44.181	473.7	47.078	325.0	48.827	(197)	45.408	415.7	48.297	243.6	49.688	(85)
350	45.90	455.5	48.184	292.7	49.76	(78)	46.77	400.1	49.28	(233)	50.51	–
400	47.11	430.4	49.00	(240)	50.52	–	47.74	377.1	50.08	(173)	51.22	
450	48.00	396.4	49.65	(139)	51.19		48.45	344.6	50.77	–	51.88	
500	48.69	349.9	50.20	–	51.82		49.01	298.9	51.39		52.52	

TABLE II. (*Continued*.)

	GaP		GaAs		GaSb		InP		InAs		InSb	
T (K)	C_p	Θ_D	C_p	Θ_D	C_p	Θ_D	C_p	Θ_D	C_p	Θ_D	C_p	Θ_D
550	49.23	(284)	50.69		52.43		49.45	(231)	52.00		53.16	
600	49.68	(174)	51.14		53.03		49.82	(100)	52.57		53.81	
650	50.06	–	51.58		53.65		50.13	–	53.16		54.48	
700	50.39		52.00		54.28		50.40		53.75		55.18	
750	50.68		52.43		54.93		50.64		54.35		55.91	
800	50.95		52.85		55.60		50.86		54.98			
850	51.19		53.29		56.30		51.07		55.62			
900	51.42		53.73		57.03		51.25		56.28			
950	51.63		54.18		57.78				56.96			
1000	51.84		54.64						57.67			
1050	53.03		55.11						58.41			
1100	52.22		55.60						59.17			
1150	52.40		56.11						59.96			
1200	52.58		56.63						60.77			
1250	52.75		57.16									
1300	52.93		57.71									
1350	53.09		58.28									
1400	53.26		58.86									
1450	43.43		59.46									
1500	53.59		60.08									
1550	53.75											
1600	53.91											
1650	54.07											
1700	54.23											

curves are rapidly falling down from their $T \to 0$ limiting levels,[45] $\Theta_D(0) = ((12/5)\pi^4 n_A R/c_3)^{1/3}$ (cf. Eq. (7)), to local minima, $\Theta_D(T_{\min})$. The latter are found to be located at certain, material-specific $T_{\min}$-positions (indicated by vertical bars, in Figs. 7 and 8), which are nearly coincident (cf. Table III) with the positions, $T_{\max}$, of the maxima, $\rho(T_{\max})$, of the respective $\rho(T)$ curves (19) (cf. the insets to Figs. 1 to 6). Thus we are obviously concerned with a close correlation between the maxima of $\rho(T)$ curves (19), on the one hand, and the minima of the respective $\Theta_D(T)$ curves (due to Eq. (20)), on the other hand.

This correlation can be described in explicit form when we take into consideration that the integrand in (20) is a rapidly (exponentially) decreasing function of the integration variable, x. Consequently, when one considers regions of sufficiently low temperatures,[23,24,27,45,65]

$$T < \Theta_D(T)/12, \tag{21}$$

one can extend in fair approximation (within an accuracy better than 1%) the range of integration to infinity, so that the integral in (20) adopts the limiting value $(2\pi)^4/15$.[23,24,43,45] Consequently, the general relationship (20) between $C_p(T)$ and $\Theta_D(T)$ reduces to the simple (algebraic) equation[43,45]

$$C_p(T) \cong (12/5)\,\pi^4 n_A R\,(T/\Theta_D(T))^3\,, \tag{22}$$

i. e. conversely

$$\Theta_D(T) \cong \left((12/5)\pi^4 n_A R/C_p(T)\right)^{1/3} \times T = \Theta_D(0)\left(c_3/C_p(T)\right)^{1/3} \times T, \tag{23}$$

(in accordance with Eq. (7)). Taking further into account that, in the cryogenic region (for $T < 30$ K, at least), the anharmonicity-related differences, $C_p(T) - C_{Vh}(T)$ (11), are throughout by factors of order 10^{-4} to 10^{-3} smaller than the respective harmonic parts, $C_{Vh}(T)$ (3), one can substitute $C_p(T)$ (in Eq. (23)) by $C_{Vh}(T)$. Thus, according to Eq. (3) and (10), one can rewrite the first version of

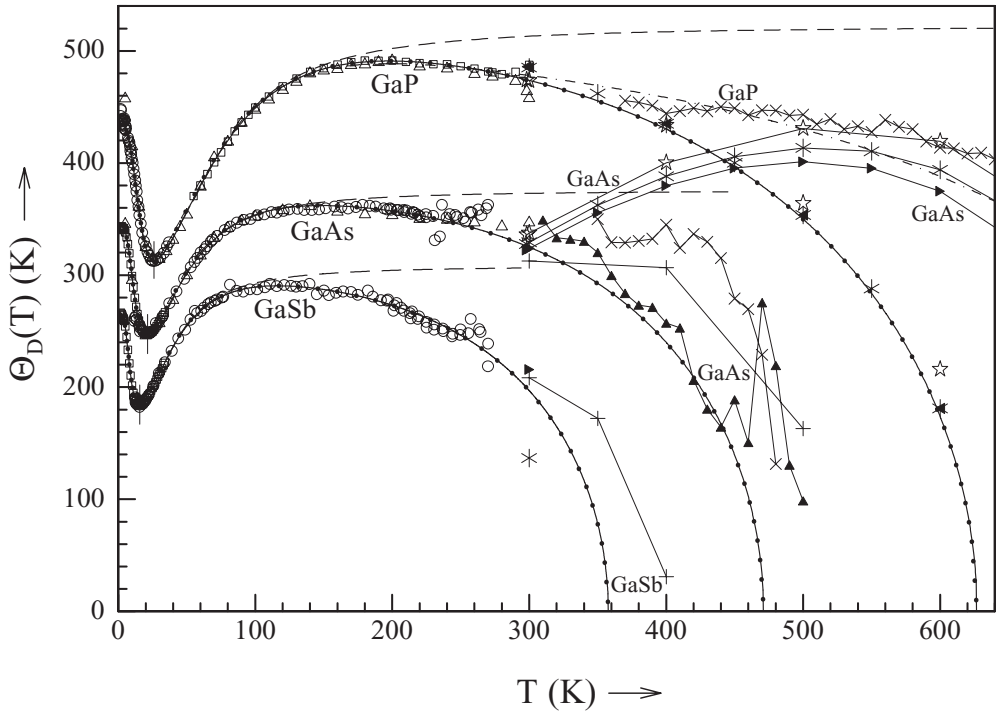

FIG. 7. Effective Debye temperatures resulting (via Eq. (20)) from $C_p^{low}(T)$ and $C_p^{high}(T)$ data available from various research papers and/or data reviews for GaP ($\Theta_D^{low}(T)$ from Refs. 54 (○), 57 (△), and 91 (□), and $\Theta_D^{high}(T)$ from Refs. 5 (☆), 6 (∗), 9 (◀), and 15 (×)), for GaAs ($\Theta_D^{low}(T)$ from Refs. 32 (□), 52 (○), and 58 (△), and $\Theta_D^{high}(T)$ from Refs. 5 (☆), 6 (∗), 12 (×), 19 (▶), 20 (+), and 93 (▲)), and GaSb ($\Theta_D^{low}(T)$from Refs. 32 (□) and 52 (○) and $\Theta_D^{high}(T)$ from Refs. 6 (∗), 19 (▶), and 20 (+)). The continuous $\Theta_D(T)$ curves (———) are resulting (via Eq. (20)) from the respective isobaric heat capacity curves, $C_p(T)$ (as shown in Figs. 1–3, respectively). Shown are also limited sections of the "true" (harmonic) Debye temperatures, $\Theta_{Dh}(T)$ (– – – –, due to Eq. (B1), and approximate $\Theta_D(T)$ curves (· · · · · · · · ·), which are resulting from a couple of complementary algebraic formulas (i. e. from Eq. (24), for $0 < T < T_{\min}$, or from Eq. (26), for $T_{\min} < T \leq T_f$).

Eq. (23) for $\Theta_D(T)$ also in the explicit form

$$\Theta_D(T) \cong \left(\frac{\frac{4\pi^4}{5}\sqrt[2]{1+\sum_{3\neq n=2}^{8} r_n(T_h)\left(\frac{T_h}{T}\right)^n + \left(\frac{3n_AR}{c_7T^7}\right)^2}}{1+\frac{c_5}{c_7T^2}+\frac{c_3}{c_7T^4}} \right)^{\frac{1}{3}} \times T. \tag{24}$$

The latter formula can be used as a welcome alternative (with respect to Eq. (20)) for calculating the decreasing sections of $\Theta_D(T)$ dependences in the cryogenic regions (see the dotted curve sections, from 0 to $T_{\min}$, in Figs. 7 and 8).

A general consequence of the very definition (Eq. (20)) of effective Debye temperatures is the fact that the calculated $\Theta_D(T)$ values are dropping to zero at those positions, T_f, where the individual $C_p(T)$ curves are crossing just the classical Delong-Petit level, i. e.

$$\Theta_D(T_f) = 0 \quad \text{for} \quad C_p(T_f) = 3n_AR, \tag{25}$$

(cf. the actual positions, T_f, of $\Theta_D \to 0$ drops of the solid $\Theta_D(T)$ curves, in Figs. 7 and 8, with the positions of crossing points (25) of the $C_p(T)$ curves, in Figs. 1 to 6). Within a detailed study of the analytical behavior of the integral (20) for the whole residual intervals, extending from the vicinity of $T_{\min}$ positions up to the T_f points (i. e. $11 > \Theta_D(T)/T \geq 0$), we succeeded here to derive

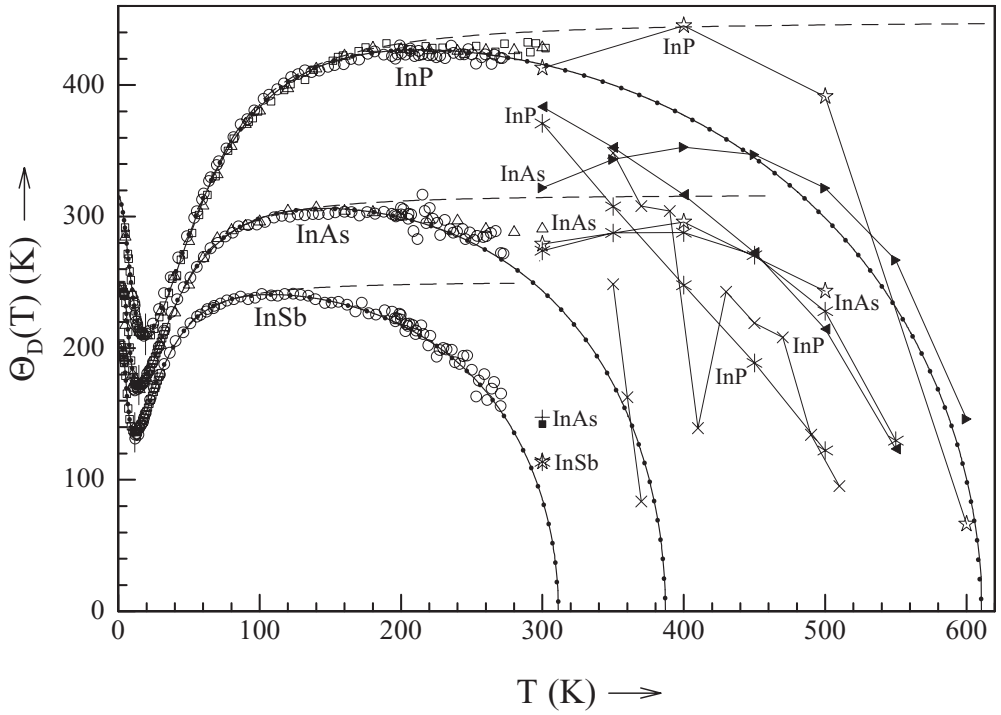

FIG. 8. Effective Debye temperatures resulting (via Eq. (20)) from $C_p^{low}(T)$ and $C_p^{high}(T)$ data available from various research papers and/or data reviews for InP ($\Theta_D^{low}(T)$ from Refs. 52 (○), 60 (△), and 94 (□), and $\Theta_D^{high}(T)$ from Refs. 5 (☆), 6 (∗), 9 (◀), and 16 (×)), for InAs ($\Theta_D^{low}(T)$ from Refs. 32 (□), 52 (○), and 60 (△), and $\Theta_D^{high}(T)$ from Refs. 4 (■), 5 (☆), 6 (∗), 13 (×), 19 (▶), 20 (+)), and for InSb ($\Theta_D^{low}(T)$ from Refs. 32 (□) and 52 (○), and $\Theta_D^{high}(T)$ from Refs. 4 (■), 5 (☆), and 6 (∗)). (Note that the associations between different curve types and the underlying analytical expressions are the same as in Fig. 7).

a largely adequate (unprecedented) algebraic expression of the relatively simple form

$$\Theta_D(T) \cong \sqrt[2]{-35+5\cdot\sqrt[2]{49+56\left(\frac{3n_AR}{C_p(T)}-1\right)}}\times T. \tag{26}$$

Note that the deviations of approximate $\Theta_D(T)$ values (due to Eq. (26)) from the exact ones (due to Eq. (20)) tend to a maximum of about 1.5% at ratios of $\Theta_D(T)/T \approx 8$ (where the $\Theta_D(T)$ curves are rapidly increasing; cf. Figs. 7 and 8). Furthermore we have found that for $4 > \Theta_D(T)/T \geq 0$, i. e. from $\Theta_{D\,\max}$ regions up to the T_f points, the corresponding deviations are even smaller than 0.3% (tending to 0 in the $T \to T_f$ limit). These findings show the potential usefulness of Eq. (26) for various practical applications. Furthermore, the $\Theta_D(T)$ curves due to Eq. (26) can be easily seen to tend (for $1 > \Theta_D(T)/T \geq 0$) to the limiting ($T \to T_f$) asymptotes

$$\Theta_D(T) \to \sqrt[2]{20\left(\frac{3n_AR}{C_p(T)}-1\right)}\times T. \tag{27}$$

We see that the individual $\Theta_D(T)$ curves, for all materials under study, are ending somewhere between 300 K and 630 K, i. e. at temperatures significantly below the melting points of these materials. This means that the very concept of effective Debye temperatures, $\Theta_D(T)$ (Eq. (20)), is largely inconvenient within the frame thermo-chemistry, which is aiming mainly to continuous analytical and numerical descriptions of thermal properties (up to melting points). On the other hand, this concept appears to be of permanent interest within the field of thermo-physics, because thermal properties in low-temperature regions are still often quantified in terms of Debye temperatures. In view of the hitherto existing lacks of comprehensive knowledge on $\Theta_D(T)$ dependences, particularly

TABLE III. Quantities manifesting the close correlation (Eq. (28) and (29)) between the general increase of $\rho(T) \equiv C_p(T)/T^3$ curves (Eq. (19); cf. the insets to Figs. 1 to 6)) from relatively low $T \to 0$ levels, $\rho(0) = c_3$, up to their local maxima, $\rho_{\max} \equiv \rho(T_{\max})$, on the one hand, and the corresponding decrease of Debye temperature curves, $\Theta_D(T)$ (Eq. (23) or (24); cf. Figs. 6 and 7), from $T \to 0$ levels, $\Theta_D(0)$, to respective local minima, $\Theta_{D\,\min} \equiv \Theta_D(T_{\min})$, on the other hand. A comparison of the magnitudes of various significant ratios between the quantities $\Theta_D(0)$, $\Theta_D(T_{\min})$, $T_{D\,\max}$, $\Theta_{D\,\max}$, T_f, and $\Theta_{Dh}(\infty)$ shows similarities of the shapes of the individual $\Theta_D(T)$ curves.

Material	GaP	GaAs	GaSb	InP	InAs	InSb
$T_{\max}$ (K)	**25.7**	**20.7**	**15.3**	**18.4**	**14.2**	**11.3**
$\rho(T_{\max})$ (μJ · K^{-4}mol^{-1})	126.1	255.8	613.0	425.4	763.1	1520.9
$\rho(0) = c_3$ (μJ · K^{-4}mol^{-1})	45.45	95.54	205.05	124.07	254.74	461.25
$\rho(T_{\max})/\rho(0)$	**2.77**	**2.68**	**2.98**	**3.43**	**3.00**	**3.30**
$(\rho(0)/\rho(T_{\max}))^{1/3}$	**0.712**	**0.720**	**0.695**	**0.663**	**0.694**	**0.672**
$T_{\min}$ (K)	**26.2**	**21.2**	**15.7**	**18.9**	**14.6**	**11.5**
$\Theta_D(T_{\min})$ (K)	312.8	247.0	184.6	208.1	171.6	136.4
$\Theta_D(T_{\min})/T_{\min}$	11.9	11.6	11.8	11.0	11.8	11.9
$\Theta_D(0)$ (K)	440.6	343.8	266.6	315.3	248.1	203.5
$\Theta_D(T_{\min})/\Theta_D(0)$	**0.710**	**0.718**	**0.692**	**0.660**	**0.692**	**0.670**
$\Theta_{Dh}(\infty)$ (K)	522	376	308	448	315	251
$\Theta_{D\,\max}$ (K)	491.0	362.1	290.5	426.8	306.2	240.8
$T_{D\,\max}$ (K)	197.8	148.2	116.3	213.8	146.6	108.2
$\Theta_{D\,\max}/T_{D\,\max}$	2.48	2.44	2.45	2.00	2.09	2.23
$\Theta_{D\,\max}/\Theta_D(0)$	1.114	1.053	1.090	1.354	1.235	1.183
$\Theta_{D\,\max}/\Theta_D(T_{\min})$	1.570	1.466	1.574	2.050	1.785	1.765
$\Theta_{Dh}(\infty)/\Theta_{D\,\max}$	1.063	1.038	1.060	1.050	1.028	1.042
T_f (K)	627	471	358	610	386	311
$T_f/\Theta_{D\,\max}$	1.28	1.30	1.23	1.43	1.26	1.29

with respect to very low temperatures ($0 < T < T_{\min}$) as well as for the relevant sections of the high-temperature region ($T_r < T \leq T_f$), we have presented here the complete $\Theta_D(T)$ curves (in Figs. 7 and 8), including a representative collection of numerical values (in Table II), for the six III-V materials under study.

B. Correlation of cryogenic non-Debye behaviors of Debye temperatures vs. heat capacities

Another useful relationship correlating the decreasing sections ($0 < T < T_{\min}$) of $\Theta_D(T)$ curves (in Figs. 7 and 8), on the one hand, with the respective increasing sections ($0 < T < T_{\max}$) of $\rho(T)$ curves (as shown in the insets to Figs. 1 to 6), on the other hand, is readily obtained by rewriting the second version of Eq. (23) in the equivalent form[43,45]

$$\frac{\Theta_D(T)}{\Theta_D(0)} \cong T\left(\frac{c_3}{C_p(T)}\right)^{\frac{1}{3}} = \left(\frac{c_3}{\rho(T)}\right)^{\frac{1}{3}} = \left(\frac{\rho(0)}{\rho(T)}\right)^{\frac{1}{3}}. \tag{28}$$

Here we have taken into consideration that, according to Eq. (8), the parameter c_3 corresponds just to the $T \to 0$ limiting value, $\rho(0)$, of the function $\rho(T) \equiv C_p(T)/T^3 \to C_{Vh}(T)/T^3$ (19). From Eq. (28) we infer, above all, that the cryogenic Debye temperature curve, $\Theta_D(T)$, can be generally expected to adopt its minimum, $\Theta_D(T_{\min})$, at the same position[43,49] on temperature scale, $T^{\Theta}_{\min} \cong T^{\rho}_{\max}$, at which the function $\rho(T)$ (19) reaches its maximum, $\rho(T_{\max})$. At the same time, due to this approximate coincidence of the minima vs. maxima positions of the two correlated functions, there follows from (28) the special relation[43]

$$\frac{\Theta_D(T_{\min})}{\Theta_D(0)} \cong \left(\frac{\rho(0)}{\rho(T_{\max})}\right)^{\frac{1}{3}}. \tag{29}$$

The latter indicates that the magnitudes of the total drops of $\Theta_D(T)$ curves, from their $T \to 0$ levels, $\Theta_D(0)$, to their minima, $\Theta_D(T_{\min})$, are unambiguously determined by the magnitudes of the total enhancements of the $\rho(T)$ curves (19), from their $T \to 0$ levels, $\rho(0) = c_3$, to the respective maxima, $\rho(T_{\max})$.

Of course, the preceding algebraic formulas for the liquid-helium-hydrogen region (i. e. Eq. (28) and (29), as well as Eq. (22) to (24)), are really valid only under the condition (21). This means that, within the whole cryogenic intervals in consideration, $0 < T < T_{\min}$, the continuously decreasing ratios, $\Theta_D(T)/T$, must be permanently larger than about 12. Accidentally, in the vicinity of the $T_{\min}$ points, these ratios are still retaining magnitudes of $\Theta_D(T_{\min})/T_{\min} \approx 11$ to 12 (cf. Table III), which are nearly equal to the critical value (lower boundary) required by condition (21). Consequently, this condition is reasonably fulfilled throughout the relevant cryogenic intervals, from 0 to the vicinities of the individual $T_{\min}$ points. This causes the obviously excellent agreement of the estimated ratios $(\rho(0)/\rho(T_{\max}))^{1/3}$ and $\Theta_D(T_{\min})/\Theta_D(0)$ with Eq. (29) (cf. Table III). At the same time we would like to underscore that these approximate equations are not applicable[43] to temperatures markedly higher than $T_{\min}$. Thus, for continuations of the $\Theta_D(T)$ curves beyond the individual $T_{\min}$ points, we have to use either the original (integral) representation (Eq. (20)) or the novel approximate expression (26).

C. Large deviations and rejection of erroneous high-temperature data

Comparing the individual sets of $\Theta_D^{low}(T)$ and $\Theta_D^{high}(T)$ points (in Figs 7 and 8), which were derived from the respective $C_p^{low}(T)$ and $C_p^{high}(T)$ data points (shown in Figs. 1 to 6), we find as a rule good agreements in the low-temperature region (from 0 up to about 250 K, at least). In contrast to this, we are concerned partly with enormous deviations of $\Theta_D^{high}(T)$ points from the smooth $\Theta_D(T)$ curves in the high temperature region. These deviations are at least partly due to the circumstance that even small uncertainties and/or moderate systematic errors of given $C_p^{high}(T)$ data are involving, according to Eq. (20) (or Eq. (26)), rather large deviations of the respective $\Theta_D^{high}(T)$ values, particularly in those regions where the $\Theta_D(T)$ curves are rapidly dropping to zero. Yet, just this apparently troublesome "blowing-up" effect for experimental uncertainties via the $C_p^{high}(T)$ to $\Theta_D^{high}(T)$ transformations has the significant advantage of showing varieties of sporadic and/or systematic errors in a much more pronounced form (in Figs. 7 and 8) than within the original $C_p^{high}(T)$ representation (in Figs. 1 to 6). As typical examples consider the sequences of the relatively low $C_p^{high(lin.)}(T)$ data points for GaAs due to Ref. 5 (☆), 6 (∗), and 19 (►). We have already disqualified these three data sets in Sec. III in view of their clear disagreement with the (somewhat sophisticated) condition (16), whose actual application assumed, naturally, a preliminary determination of the harmonic part, $C_{Vh}(T)$, via a preceding fit of $C_p^{low}(T)$ data sets. In contrast to this we see now immediately from the graphical representations of the respective $\Theta_D^{high}(T)$ points in Fig. 7 that these three sequences deviate in rather drastic way from the overall behavior of the $\Theta_D(T)$ dependence for GaAs. In particular we see that these three sequences tend to an obviously unrealistic (second maximum) behavior in the vicinity of 500 K, whereas the physically realistic $\Theta_D(T)$ curve dropped already to 0 at about 470 K. Furthermore we see that the fictitious maximum values, of about $\Theta_{D\,\max} \approx 400$ K to 430 K, are even exceeding the well established $T \to \infty$ limiting value of $\Theta_{Dh}(\infty) = 376$ K. This is impossible from physical points of view (cf. the detailed analysis of the $\Theta_D^{low}(T)$ data sets in Appendix B).

Analogously we see from Fig. 8 that three sequences of $\Theta_D^{high}(T)$ points for InAs, which are representing the $C_p^{high(lin.)}(T)$ data sets due to the same sources as the aforementioned ones for GaAs (namely Refs. 5 (☆), 6 (∗), and 19 (►)), show the same type of characteristic deficiencies. These sequences show, again, an obviously unrealistic (second maximum) behavior in the vicinity of 400 K, whereas the physically realistic $\Theta_D(T)$ curve dropped to 0 just in this region. In this way, the $\Theta_D^{high}(T)$ representations provide striking additional arguments for definitive rejections of the $C_p^{high(lin.)}(T)$ data sets due to Refs. 5 (☆), 6 (∗), and 19 (►), both for GaAs and InAs.

Finally we are concerned also with a largely atypical behavior (namely an unusually weak decrease) of the sequence of $\Theta_D(T)$ values due to Ref. 15 (×) for GaP (see the double-dashed-dotted

curve in Fig. 7). Moreover we see from Fig. 1 that the fictitious double-dashed-dotted curve, which is due to a tentative fit of the $C_p^{high}(T)$ data points given in Ref. 15 (×) in combination with those available for $T \geq 800$ K from Ref. 10 (◊), crosses the classical Dulong-Petit level at $T_f \approx 860$ K. This would mean, in view of a given maximum value of $\Theta_{D\,\max} = 491$ K (cf. Fig. 7 and Table III), an apparent $T_f/\Theta_{D\,\max}$ ratio of 1.75. The latter value is by about 35% higher than the typical magnitude of these ratios for the III-V materials under study (cf. Table III). The $C_p^{high}(T)$ data due to Ref. 10 (◊) and 15 (×) would thus imply a largely atypical shape of the whole $\Theta_D^{high}(T)$ curve section. These indications might be sufficient for considering also the latter $C_p^{high}(T)$ data sets as physically rather unrealistic ones. A definitive conclusion in this respect, however, can not be made unless more accurate $C_p^{high}(T)$ data become available for GaP.

V. DISCUSSION

We have established in this paper a refined version (10) of a recently proposed non-Debye heat capacity formula[37] which, in combination with the duly general formula (11) for the anharmonicity-related differences of isobaric vs. isochoric (harmonic) heat capacities, turned out to be capable of providing fine numerical descriptions of comprehensive $C_p(T)$ data sets for several III-V materials, from the cryogenic region up to melting points. An important feature of this representative analytical framework (displayed Sec. II) is due to its readiness for applications to materials with largely different phonon spectra. Of particular value is its general capability of describing in adequate way the commonly observable non-Debye behaviors of $C_p(T)$ data in the cryogenic region. This has been clearly shown here by the fine numerical simulations of the non-monotonic (local maximum) behaviors of combinations of several compatible $\rho(T) = C_p(T)/T^3$ data sets, the most informative components of which are due to the $\Theta_D(T)$ data points given for GaP in Ref. 54 (cf. Fig. 1) and the very detailed $C_p(T)$ data sets given for GaAs, GaSb, InAs, and InSb in Ref. 32 (cf. Figs. 2, 3, 5, and 6, respectively) or for InP in Ref. 94 (cf. Fig. 4).

Approximate simulations of comparable $C_p(T)/T^3$ data sets have been performed in last years also as inherent parts of studies of isotopic effects in several group-IV[33–35] and II-VI[36,39–42] materials. The novel non-Debye heat capacity formula (10) might thus be useful in future also as an effective analytical tool for fine numerical simulations of varieties of $C_p(T)/T^3$ data sets available for isotopically modified samples.

A. Important role of conveniently chosen scaling temperatures

A practicable way for ready applications of the present analytical framework to a series of materials with largely different extensions of PDOS spectra (cf. the individual $\varepsilon_{Dh}(\infty)$ values quoted in Table V) was found to be given via the introduction of conveniently chosen scaling temperatures (in particular by $T_s = T_h$, in Eq. (10)). In general one can state that that a substitution of the preceding set of expansion coefficients, ρ_n (occurring in the denominator of Eq. (A3)), by products of certain T_s^n power terms multiplied with dimensionless, T_s-related coefficients, $r_n(T_s)$, has the advantage that one has a good chance to be concerned in numerical applications as a rule with only moderate, material-specific changes of magnitudes of the respective expansion coefficients, $r_n(T_s)$ ($n = 2$, and 4 to 8), provided that the T_s values adopted for different materials are roughly proportional to the actual extensions (e. g. upper boundaries, $\approx \varepsilon_{Dh}(\infty)$) of the respective PDOS spectra. This global requirement would be fulfilled by choosing T_s to be equal, e. g., to the $T \to \infty$ limits of the Debye temperature, $\Theta_{Dh}(\infty)$ (for the harmonic lattice regime; cf. Appendix B). However, owing to the relatively high magnitudes of $\Theta_{Dh}(\infty)$ values (see Table V), the magnitudes of the respective expansion coefficients, $r_n(T_s \to \Theta_{Dh}(\infty))$, turned out to decrease very rapidly (even by orders of magnitude) with increasing n. Fortunately, such rapid drops of $r_n(T_s)$ values with increasing order, $n = 2$ to 8, could be generally be avoided by choosing the scaling temperatures, T_s, to be coincident with those characteristic points on T-scale, T_h (Eq. (9)), where the measured $C_p(T)$ values are adopting a magnitude of just 50% of the classical Dulong-Petit value, i. e. $C_p(T_h) = C_{Vh}(\infty)/2$

(cf. Eq. (9) and see Figs. 1 to 6). Due to this particular choice, $T_s = T_h$ (as indicated by bold numbers in Table I), the orders of magnitude of several expansion coefficients follow automatically to be comparable with unity, $r_n(T_h) \approx 10^0$ (for $n = 2$ and 4 to 6, at least). Moreover, it is an immediate consequence of this particular choice (as briefly discussed in the Appendix A) that the sum of the whole set of the 6 expansion coefficients should be approximately equal to 3 (cf. Eq. (A4)). Indeed, we see from the parameter values listed in Table I that marked deviations (up to an order of 5%) of the sums (A4) from the ideal value (of 3) are encountered only for GaP and InP, whereas the deviations for GaAs, GaSb, InAs, and InSb are even limited to an order of 1%.

Another characteristic feature of the fitted sets of $r_n(T_h)$ values consists in their alternating signs for the orders $n = 4$ to 8. Actually, we see from Table I that, for all materials under study, the even-order coefficients are positive, whereas the odd-order coefficients are throughout negative. It is this alternating character of the sequences of the five subsequent expansion coefficients ($n = 4$ to 8) which is the main cause of significant refinements of the numerical simulations of given $C_p(T)$ data sets by means of the present non-Debye interpolation formula (Eq. (10)), in comparison with somewhat rougher fittings by the original version[37] (i. e. Eq. (A1) or (A3)).

Furthermore we see from Table I that the magnitudes of the expansion coefficients, $r_n(T_h)$, of the individual orders ($n = 2$ and 4 to 8), are changing only moderately (by factors not exceeding an order of 3) from one material to the other. This is a highly convenient property which enables us, e. g., in the frame of sequential simulations of $C_p(T)$ data sets for several materials, to employ a preceding set of fitted $r_n(T_h)$ values as usable starting values for subsequent least-mean-square processes (provided, of course, that adequate values for the material-specific T_h positions (9) have been adopted in Eq. (10)).

B. Efficient version of least-mean-square fitting processes

We see from Table I that, in contrast to the order-of-magnitude equalities of the $r_n(T_h)$ coefficients, the magnitudes of the characteristic low-temperature expansion coefficients, c_3, c_5, and c_7, are changing rather strongly (even in their orders of magnitude) from one material to the other. Approximate (starting) values for c_3 can be readily estimated via Eq. (7) on the basis of limiting $\Theta_D(0)$ values (the magnitudes of which use to be known for numerous materials). Reasonable starting values for the other two low-temperature parameters, c_5 and c_7, can be estimated, e. g., by means of conventional analysis procedures[29,31,45] for cryogenic $C_p(T)$ data sets. However, such provisional c_5 and c_7 values use to undergo strong changes during the subsequent fitting processes for the whole $C_p(T)$ curves. In order to come in effective way to an unambiguous, final constellation of adjusted values for the complete parameter set it turned out to be mandatory to endow the low-temperature data with significantly higher weights[74,96] than the high-temperature data. We have found that an adequate way for duly different weightings of the individual experimental heat capacity values, $C_p^{ex.}(T_i)$, is given by weighting factors, W_i, which are inversely proportional to their squares,[74,96] i. e. $W_i \propto (C_p^{ex.}(T_i))^{-2}$. The actual aim of the least-mean-square fitting processes within the present context consisted thus in minimizations of sums of type,[74,96]

$$\sum_i W_i \left(C_p^{th.}(T_i) - C_p^{ex.}(T_i)\right)^2 \propto \sum_i \left(\frac{C_p^{th.}(T_i) - C_p^{ex.}(T_i)}{C_p^{ex.}(T_i)}\right)^2 \rightarrow \min., \tag{30}$$

where we have denoted by $C_p^{th.}(T_i)$ the theoretical heat capacity values for the individual T_i-points (as resulting from Eq. (12) in combination with (10)). Properly speaking, this special choice of weighting factors corresponds to a minimization of the sums of squares just of the relative deviations, $\propto (C_p^{th.}(T_i)/C_p^{ex.}(T_i) - 1)^2$, between experimental and theoretical $C_p(T_i)$ values. This version of the least-mean-square minimization procedure is consistent with the well known fact that the relative deviations from smoothed curves are as a rule nearly constant (of order 0.5%), from the cryogenic region up to room temperature (whereas the absolute values of deviations are automatically tending to 0 in the $T \rightarrow 0$ limit).

C. Rough estimations of limiting Debye temperatures for the harmonic regime

In contrast to the aforementioned advantages of the present analytical framework, which is basing essentially on the refined non-Debye interpolation formula (10), it appears necessary to indicate also an inherent shortcoming of this model (in comparison e. g. with multi-oscillator hybrid models).[43,50,74] This is due to the circumstance that the magnitudes of material-specific PDOS spectral moments,[43] $\mu_P^{(m>-3)}$, can not directly be derived from the fitted sets of the parameters occurring in Eq. (10) (Table I). This deficiency concerns also estimations of a frequently quoted moment-related quantity like the $T \to \infty$ limiting Debye temperatures, $\Theta_{Dh}(\infty)$ (cf. Table V), which are known to be generally connected with the second moments by the relation[29,31,43,50] $\Theta_{Dh}(\infty) = \sqrt[2]{(5/3)\mu_P^{(2)}}/k_B$ (cf. Eq. (B3a)). In terms of the latter, one can represent the high-temperature asymptote (5) of the $\kappa_P(T)$ function in the equivalent form

$$\kappa_P(T) \to 1 - \frac{(\Theta_{Dh}(\infty))^2}{20T^2}. \tag{31}$$

On the other hand, the presently used non-Debye formula (10) for $\kappa_P(T)$ functions tends in the high-temperature limit to the asymptote

$$\kappa_P(T) \to 1 - \left(\frac{r_2(T_h)T_h^2}{2} - \frac{c_5}{c_7}\right)\frac{1}{T^2}. \tag{32}$$

Comparing (32) with (31) one can conclude that limiting Debye temperatures, $\Theta_{Dh}(\infty)$, should be given in terms of the presently estimated parameters by

$$\Theta_{Dh}(\infty) = \sqrt[2]{10\left(r_2(T_h)T_h^2 - 2c_5/c_7\right)} \cong \sqrt[2]{10r_2(T_h)} \times T_h. \tag{33}$$

(Note that, according to the parameter sets listed in Table I, the $2c_5/c_7$-terms are throughout by orders of magnitude lower than the largely dominating $r_2(T_h)T_h^2$ terms.) Using, tentatively, the latter expression we obtain from the couples of the fixed T_h positions in combination with the respective $r_2(T_h)$ values (listed in Table I) for the limiting Debye temperatures, $\Theta_{Dh}(\infty)$, the following values: 491 K for GaP, 359 K for GaAs, 285 K for GaSb, 448 K for InP, 320 K for InAs, and 244 K for InSb. Comparing these approximate $\Theta_{Dh}(\infty)$ values with their more reliable counterparts listed in Table V (cf. also Table B1 in the supporting information to Ref. 74) we find relatively good agreements (within deviation up to 3%) for InP, InAs, and InSb. In contrast to this, we are concerned for GaP, GaAs, and GaSb with relatively large deviations (underestimations ranging between 4% and 8%). Thus the presently used non-Debye interpolation formula (10) is obviously not well suited for accurate determinations of high-temperature limiting Debye temperatures. (Note that the same statement applies also to the original version[37] of the non-Debye interpolation formula).

D. Qualitatively different shapes of high temperature heat capacity curves

A crucial feature of the present analytical framework (Sec. II) is its adaptability to qualitatively different (i. e. concave vs. convex) curve shapes in the high temperature region. This changeability of material-specific curve shapes is due to the considerable variability of the weights of quadratic ($\propto A_2T^2$) vs. linear ($\propto A_1T^1$) components, which are determining the actual shapes of the anharmonicity-related heat capacity differences, $C_p(T) - C_{Vh}(T) > 0$ (Eq. (11)). The corresponding temperature dependences, which are following from the results (Table I) of the fittings in Sec. III, are shown in Fig. 9. From the latter we see, first of all, that the magnitudes of these differences, as well as the slopes of the individual $C_p(T) - C_{Vh}(T)$ curves above room temperature (up to about 800 K, at least) are significantly increasing, both for the Ga-group-V and for the In-group-V materials, with increasing anion masses. Moreover we see that these curves reveal a pronounced qualitative difference between the arsenides and antimonides, on the one hand, and phosphides, on the other hand. Concerning the latter we see that the anharmonicity-related differences $C_p(T) - C_{Vh}(T) > 0$ are comparatively small, and their T-dependences are nearly linear. Consequently, their combination (12) with the inherently convex dependences of the harmonic parts, $C_{Vh}^{high}(T)$, does not alter the

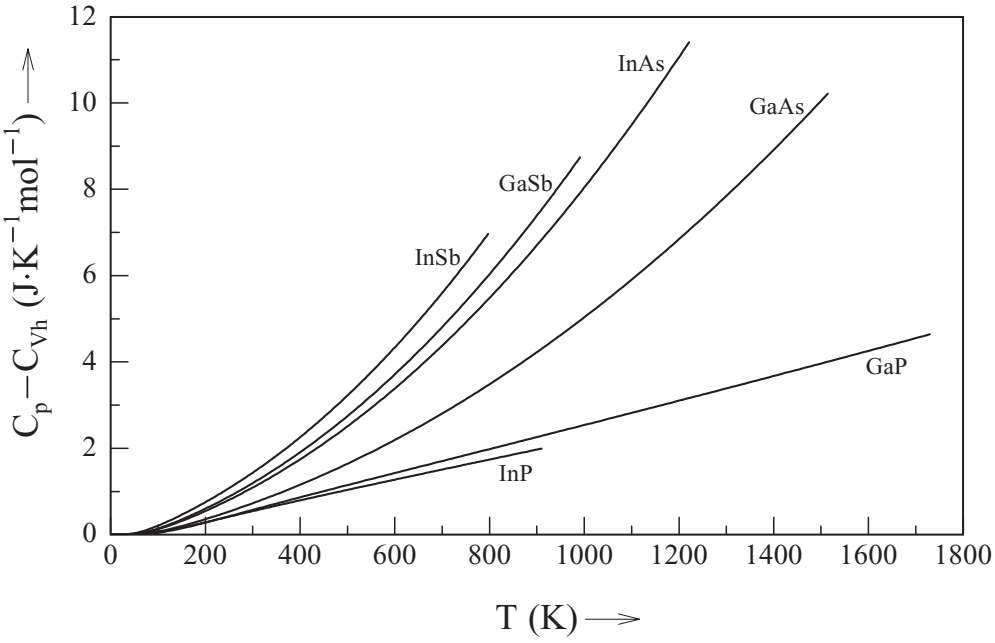

FIG. 9. Temperature dependences of the anharmonicity-related differences of isobaric vs. isochoric (harmonic) heat capacities, $C_p(T) - C_{Vh}(T)$, which are resulting (via Eq. (11), in combination with Eq. (10)), from the parameter values quoted for the six cubic III-V materials under study in Table I.

curvatures of the latter. This explains the exclusively convex shape of the resulting $C_p^{high}(T)$ curves, both for GaP (Fig. 1) and for InP (Fig. 4). In contrast to this, the $C_p(T) - C_{Vh}(T)$ dependences for GaAs, InAs, GaSb, and InSb are seen from Fig. 9 to be obviously strongly governed by quadratic terms. The inherently concave behaviors of the latter are so pronounced that they are even capable of overcompensating the convex behaviors of the associated harmonic parts, $C_{Vh}^{high}(T)$. This explains the change of the curvatures (snake-like behaviors) of the resulting $C_p^{high}(T)$ curves from convex shape (at $T \approx T_r$) to a more or less pronounced concave shape in the upper parts of the high temperature region, for GaAs (Fig. 2), GaSb (Fig. 3), InAs (Fig. 5), and InSb (Fig. 6). On the other hand, it can not be excluded that in some special case the concave vs. convex shape compensation effects are accidentally such that the shape of the resulting $C_p^{high}(T)$ curve changes from convex behavior (at $T \approx T_r$) to an approximately linear one (close to the melting point). Accordingly, for such a special state of affairs, the respective $C_p^{high}(T)$ dependence would have a chance to be satisfactorily simulated even by the simple Maier-Kelley equation (1). However, a definitive discrimination between concave, nearly linear, and/or convex shapes of the upper parts of $C_p^{high}(T)$ curves (close to melting points) can hardly be made at present in view of the excessive scarcity and uncertainty of most high-temperature heat capacity and/or enthalpy data which are available hitherto for III-V materials (including many other binary and ternary materials, too).

VI. IMPROVED HIGH-TEMPERATURE POLYNOMIAL REPRESENTATION AND NOVEL RESULTS

Concerning the high-temperature parts of isobaric heat capacities, $C_p^{high}(T)$, we were concerned here continually with the notorious problem[12–17] of the occurrence of rather large discrepancies for III-V compounds. Unusually large differences (up to an order of 10%, in the vicinity of melting points) have been found in particular between the $C_p^{high}(T)$ values quoted by different authors and/or in different data reviews for GaAs (cf. Fig. 2) and InAs (cf. Fig. 5). Fortunately, on the basis of the criterion (16) we were able to reject several $C_p^{high}(T)$ data sets as obviously erroneous ones. This concerned above all those given in Ref. 4, for GaP, and in Refs. 5, 6 and 19, for GaAs and InAs.

Incisive additional arguments supporting the definitive rejection of these data sets were provided (in Subsection IV C) in face of the excessively large deviations of the respective Debye temperature points, $\Theta_D(T)$ (shown in Figs. 7 and 8), from common trends. Furthermore, in view of an extremely weak decrease of the fictitious $\Theta_D(T)$ curve due to Refs. 10 and 15 for GaP (double-dashed-dotted curve in Fig. 7), this apparent alternative for the $C_p^{high}(T)$ behavior of GaP could also be assessed as a physically hardly realistic one. On the other hand, it was not possible to exclude several residual uncertainties, especially for GaAs and InAs, which are inherent to hitherto available literature data. The corresponding uncertainty ranges are indicated by the bifurcations between the upper and lower double-dashed-dotted curves, which were due to tentative alternative fittings of qualitatively more or less different $C_p^{high}(T)$ data sets, namely those of Ref. 12 vs. 20 for GaAs, in Fig. 2, and those of Ref. 4 vs. 20 for InAs, in Fig. 5. These bifurcations are visualizing a rapid increase of uncertainties with increasing temperature. We see that, close to the melting points, the residual uncertainties are reaching an order of about 3 J/(Kmol) (i. e. nearly 5%) for GaAs and about 6 J/(Kmol) (i. e. nearly 10%) for InAs.

Particularly in view of the excessively large residual uncertainty for InAs we would like to make here still an attempt to re-evaluate some genuine experimental data for enthalpy differences, $\Delta H_p(T) \equiv H_p(T) - H_p(T_r)$, that are available in graphical form from Refs. 10 and 20, for GaAs and InAs. An improved numerical analysis of such $\Delta H_p(T)$ data requires, of course, a more appropriate analytical model than those ones used in former enthalpy research papers.

A. Construction of an improved high-temperature polynomial representation

In order to establish an improved analytical model for high-temperature data analyses, we take into considerations the following points of view. Firstly, it is well know from Thirring's global high-to-intermediate-temperature representation[85] that the harmonic parts of heat capacities can be represented in general by a Taylor series consisting exclusively of T^{-2n}-power terms,

$$C_{Vh}^{high}(T) = C_{Vh}(\infty) - C_{-2}/T^2 + C_{-4}/T^4 - ..., \tag{34}$$

where the constant (a priori fixed) term is just coincident with the classical Dulong-Petit limit, $C_{Vh}(\infty) = 3n_A R$, and the subsequent two lowest-order expansion coefficients are given in terms of the corresponding even-order moments[24,29,50,82,85] of the individual PDOS spectral functions, $\mu_P^{(2)}$ and $\mu_P^{(4)}$, by the relations $C_{-2} = C_{Vh}(\infty)\mu_P^{(2)}/12(k_B)^2$ and $C_{-4} = C_{Vh}(\infty)\mu_P^{(4)}/240(k_B)^4$. Secondly, for the anharmonicity-related differences (11) in the high-temperature region, one can substitute the characteristic low-temperature reduction factor in roughest approximation by its $T \to \infty$ limiting value, $(\kappa_p(T \to \infty))^2 = 1$. In this way we reduce (11) to the simplified form[50,92]

$$C_p^{high}(T) - C_{Vh}^{high}(T) = C_1 T + C_2 T^2 + ..., \tag{35}$$

(where $C_n \cong C_{Vh}(\infty)A_n, n = 1, 2, \ldots$). Lumping, henceforth, the components (34) and (35) together, we come thus to a high-temperature expression for isobaric heat capacities of the special form

$$C_p^{high}(T) = C_{Vh}(\infty) - C_{-2}/T^2 + C_{-4}/T^4 + C_1 T + C_2 T^2. \tag{36}$$

In order to verify the actual degree of usability of this high-temperature polynomial we have performed test fittings of large sequences of the pre-calculated $C_p(T)$ values (listed in Table II), which resulted from the primary fittings by means of the original $C_p(T)$ formula (Eq. (12)). The readjusted $C_p^{high}(T)$ curves due to Eq. (36) are shown in Figs. 10 and 11, and the respective quadruples of empirical parameter values are listed in Table IV. We have found that, within the respective T-intervals (indicated in Table IV), the readjusted $C_p^{high}(T)$ curves are practically indistinguishable from the original $C_p(T)$ curves shown in Figs. 1 to 6. (Note that the differences between original $C_p(T)$ values and the readjusted ones, $C_p^{high}(T)$, are throughout smaller than 0.05%).

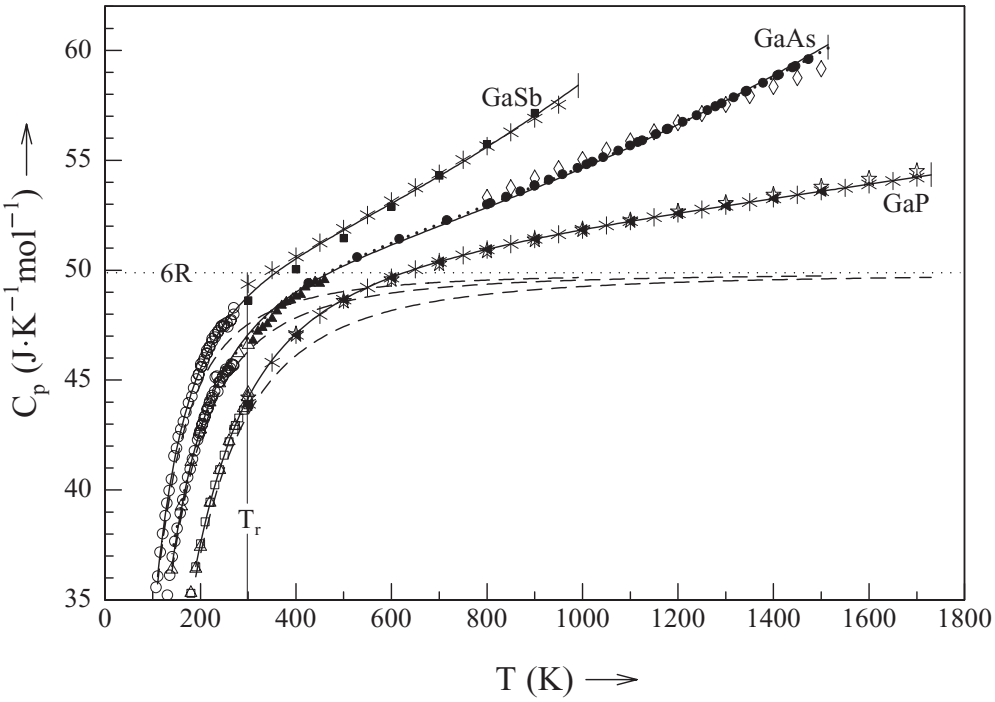

FIG. 10. Reproduction of upper sections of the previously determined $C_p(T)$ and $C_{Vh}(T)$ curves, for GaP, GaAs, and GaSb (cf. the solid and dashed curves, in Figs. 1 to 3), by means of the properly devised polynomials, i. e. Eq. (36) for $C_p^{high}(T)$ (———) and Eq. (34) for $C_{Vh}^{high}(T)$ (- - - -), with coefficients quoted in Table IV. (Symbols for selected data are the same as in Figs. 1 to 3.)

B. Joint fittings of heat capacity and enthalpy data for GaAs and InAs

The obviously excellent functioning of Eq. (36) for reproductions of given $C_p(T)$ dependences encouraged us to use this formula also as a basis for possible re-evaluations of enthalpies (29). Performing the corresponding integration one obtained readily (exactly) for the relevant enthalpy differences a polynomial expression of the form

$$H_p^{high}(T) - H_p(T_r) = C_{Vh}(\infty)\,(T - T_r) + C_{-2}\left(T^{-1} - T_r^{-1}\right) - C_{-4}\left(T^{-3} - T_r^{-3}\right)/3 + \\ + C_1\left(T^2 - T_r^2\right)/2 + C_2\left(T^3 - T_r^3\right)/3. \qquad (37)$$

The couple of these novel, self-consistent heat capacity and enthalpy expressions (i. e. Eqs. (36) and (37)) can be used, e. g., in the following way. Fitting first a duly truncated (upper) section of low-temperature heat capacity data, $C_p^{low}(T) > 0.8 \cdot C_{Vh}(\infty)$, by means of Eq. (36), one obtains preliminary values for the coefficients C_{-2}, C_{-4}, and C_1. Using the latter in Eq. (37) one can adjust the parameter C_2 by fitting the given enthalpy differences, $H_p(T_i) - H_p(T_r) > 0$, from which follows readily a corresponding series of provisional $C_p^{high}(T_i)$ data points via the first derivative of Eq. (37) (i. e. via Eq. (36)). The latter $C_p^{high}(T_i)$ data can then be used, in combination with the given low-temperature data set, $C_p^{low}(T)$, for a novel (complete) fit via Eq. (36). Performing, if necessary, several cycles of such alternating fitting processes for heat capacity and enthalpy data one has a good chance of reaching a stabilization of the whole set of the 4 empirical parameters.

Using, accordingly, some former enthalpy data available in graphical form for GaAs[10,20] and for InAs,[20] we have derived in this way novel, self-consistent sets of $C_p^{high}(T_i)$ data points. These are represented by solid circles (●) in Figs. 2 and 10 (for GaAs) and in Figs. 5 and 11 (for InAs). It is remarkable that, particularly the novel set of $C_p^{high}(T_i)$ data points for GaAs, shows a rather pronounced concave behavior[18] in the region from 800 K up to the melting point. This is in analogy

TABLE IV. Adjusted magnitudes of the empirical parameters involved by the presently devised polynomial (36), which provided an accurate reproduction (shown in Figs. 10 and 11) of upper sections, $C_p(T) > 0.8 \cdot C_{Vh}(\infty)$, of the previously fitted $C_p(T)$ curves (cf. Figs. 1 to 6).

	GaP	GaAs	GaSb	InP	InAs	InSb
intervals (K)	190 to 1730	140 to 1514	110 to 991	200 to 910	130 to 1221	110 to 797
C_{-4} (J · K^3/mol)	4.8571×10^9	1.3578×10^9	5.5329×10^8	3.9538×10^9	1.1300×10^9	3.3116×10^8
C_{-2} (J · K^1/mol)	6.3373×10^5	3.3667×10^5	2.1701×10^5	5.0411×10^5	2.6205×10^5	1.5497×10^5
C_1 (J/(K^{2}mol))	2.4292×10^{-3}	1.4663×10^{-3}	2.2826×10^{-3}	2.0781×10^{-3}	2.1265×10^{-3}	2.6561×10^{-3}
C_2 (J/(K^{3}mol))	1.5084×10^{-7}	3.6197×10^{-6}	6.6068×10^{-6}	1.4272×10^{-7}	5.9200×10^{-6}	7.6558×10^{-6}

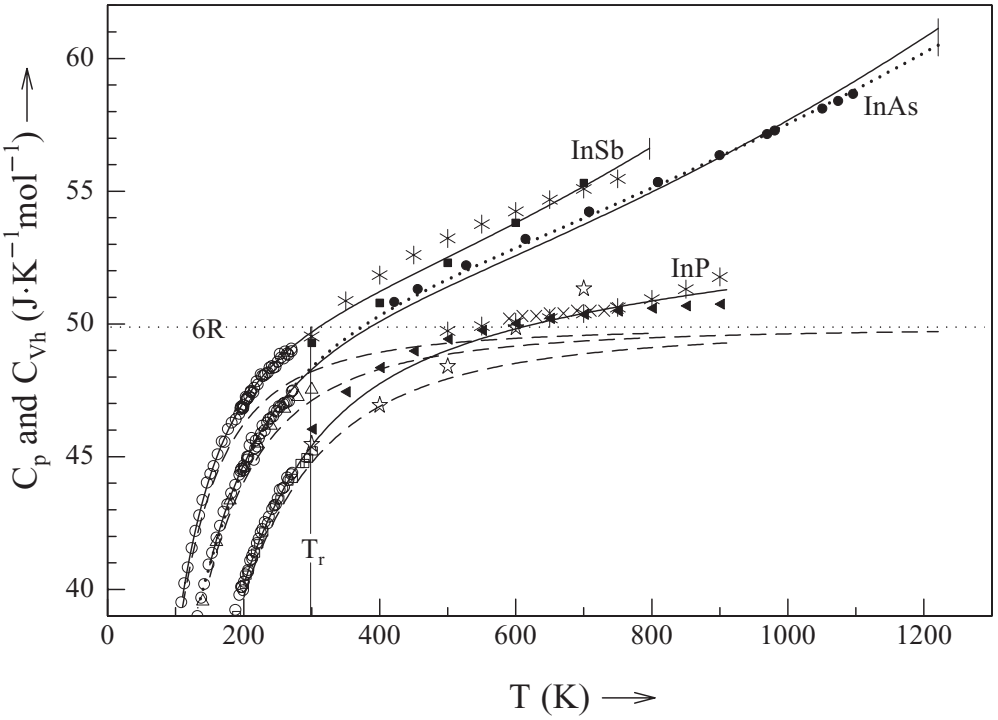

FIG. 11. Reproduction of upper sections of the previously determined $C_p(T)$ and $C_{Vh}(T)$ curves, for InP, InAs, and InSb (cf. the solid and dashed curves, in Figs. 4 to 6), by means of the properly devised polynomials, i. e. Eq. (36) for $C_p^{high}(T)$ (———) and Eq. (34) for $C_{Vh}^{high}(T)$ ((- - - - -), with coefficients quoted in Table IV. (Symbols for selected data are the same as in Figs. 4 to 6.)

to the concave shapes of the high-temperatures sections ($T > 400$K) of the fitted $C_p(T)$ curves for GaSb (Fig. 10) and InSb (Fig. 11). On the other hand we see also from Fig. 11 that the novel set of $C_p^{high}(T_i)$ data points for InAs is tending to a nearly linear dependence, from 400 K up to the melting point. This approximate linearity is apparent in particular from the dotted curve shown for InAs (in Fig. 11), which represents the direct result of the iterative fitting procedure sketched above.

VII. SUMMARY

It was the main aim of this paper to provide comprehensive analytical and numerical descriptions of the temperature dependences of isobaric heat capacities of several III-V materials over unusually broad temperature intervals, beginning from absolute zero up melting points. The analytical basis for the respective least-mean-square fittings was given by a refined version (Eq. (10)) of the recently proposed non-Debye heat capacity formula[37] (cf. the Appendix A), in combination with a duly general formula[43,50,74,82] (Eq. (11)) for the anharmonicity-related differences of isobaric vs. isochoric

(harmonic) heat capacities. The fittings in the high-temperature region were significantly impeded by the notorious circumstance that the data sets quoted in different research papers and/or data reviews differed in many cases significantly from one another (up to an order of 10%). Therefore we have invoked several, physically plausible criteria (in Sec. III and IV), on the basis of which we were able to exclude a priori a variety of obviously inadequate data sets from further considerations. Furthermore we have devised (in Sec. VI) a physically adequate couple of four-parameter polynomial equations for heat capacities and enthalpies within regions of intermediate to high temperatures, by means of which we could estimate in self-consistent way novel, high-temperature heat capacity values for GaAs and InAs.

Representative sets of isobaric heat capacity values for the whole temperature ranges of interest (i. e. from the liquid-helium region up to the vicinity of melting points), that resulted from the comprehensive least-mean-square fitting processes in Sec. III, are listed in Table II. An important novel aspect of the heat capacity behaviors in the high-temperature region are the more or less pronounced snake-like shapes (changes from convex to concave shape) both for arsenides (Fig. 10) and antimonides (Fig. 11). These refined results might be suitable for being eventually taken into consideration within forthcoming editions of high-temperature data reviews.[4–6] At the same time we would like to point out that moderate modifications of heat capacity values up to about ±2 J/(Kmol), for very high temperatures (close to melting points), should be envisaged at the prospective of more comprehensive and accurate experimental heat capacity and/or enthalpy data that might become available in future.

APPENDIX A: TRANSFORMATION AND REFINEMENT OF THE CHARACTERISTIC NON-DEBYE HEAT CAPACITY FORMULA

It had been shown in Ref. 37 that the harmonic parts (3) of lattice heat capacities can be simulated in good approximation by a low-to-high-temperature interpolation formula of type

$$C_{Vh}(T)=\frac{c_3T^3+c_5T^5+c_7T^7}{\sqrt[2]{1+\sum_{n=3}^{6}\beta_{2n}T^{2n}+\left(\frac{c_7T^7}{3n_AR}\right)^2}}\equiv\frac{c_3T^3+c_5T^5+c_7T^7}{\sqrt[2]{1+\sum_{n=3}^{7}b_{2n}(T_o)\left(\frac{T}{T_o}\right)^{2n}}},\tag{A1}$$

where β_{2n} (for n =3, 4, 5, and 6) and c_{3+2n} (for n =0, 1, and 2; cf. Eq. (6)) are empirical parameters, which are to be adjusted in the course of least-mean-square fitting processes. (Note that the second representation of Eq. (A1), which is just identical with Eq. (2) of Ref. 37, involves an arbitrarily chosen scaling temperature, T_o, with respect to which the corresponding expansion coefficients,[37] $b_{2n}(T_o)=\beta_{2n}T_o^{2n}$ (n = 3 to 6) and $b_{14}(T_o)=\left(c_7T_o^7/3n_AR\right)^2$, are dimensionless quantities.)

Multiplying now both the numerator and the denominator by the factor $3n_AR/c_7T^7$ one can rewrite the $C_{Vh}(T)$ formula (A1) in the usual product form (10),

$$C_{Vh}(T)=3n_AR\kappa_P(T),\tag{A2}$$

where the respective (normalized) heat capacity shape function is given by

$$\kappa_P(T)=\frac{\frac{c_3}{c_7T^4}+\frac{c_5}{c_7T^2}+1}{\sqrt[2]{\left(\frac{3n_AR}{c_7T^7}\right)^2+\sum_{n=3}^{6}\left(\frac{3n_AR}{c_7}\right)^2\frac{\beta_{2n}}{T^{14-2n}}+1}}\equiv\frac{1+\frac{c_5}{c_7T^2}+\frac{c_3}{c_7T^4}}{\sqrt[2]{1+\sum_{m=1}^{4}\frac{\rho_{2m}}{T^{2m}}+\left(\frac{3n_AR}{c_7T^7}\right)^2}}.\tag{A3}$$

The latter representation of the $\kappa_P(T)$ function (A3) is due to an introduction of transformed expansion coefficients, ρ_{2m}, which are given in terms of the original ones, β_{2n}, by the definition $\rho_{2m}\equiv(3n_AR/c_7)\,\beta_{14-2m}$ (m = 1, 2, 3, and 4).

A characteristic feature both of the original and of the transformed versions (i. e. Eq. (A1) and (A3)) of analytical $C_{Vh}(T)\propto\kappa_P(T)$ formulae is the occurrence of exclusively even-order power terms of the temperature in the respective denominators (i. e. $\propto T^{2n}$-terms, n = 3 to 7, in (A1), or $\propto T^{-2m}$-terms, m =1 to 4 and 7, in (A3)). Notwithstanding the fact that such 7-parameter versions are already capable of providing relatively good simulations of $C_{Vh}(T)\propto\kappa_P(T)$

functions (as it had been shown e. g. for GaN and ZnO in Ref. 37), we have made within the present study the observation that further refinements of numerical simulations, particularly within the liquid-hydrogen-nitrogen region, can be readily achieved when we admit the incorporation of two additional odd-order power terms (namely $\propto T^{-5}$ and $\propto T^{-7}$ terms) in Eq. (A3). Furthermore we have introduced (in analogy to Ref. 37) convenient (material-specific) scaling temperatures, T_s, by their identification with the characteristic (easily detectible) temperature points, T_h (Eq. (9)), at which the individual $C_p(T)$ curves are reaching just 50% of the classical Dulong-Petit value. In this way we came finally to the refined (9-parameter) $\kappa_P(T)$ expression (Eq. (10)) used in the present paper.

Let us still make some useful remarks concerning the present (apparently optimum) choice (9) for the scaling temperatures, $T_s^{(fixed)} = T_h$, with respect to practical applications of Eq. (10). If one would adopt one and the same T_s value for a larger variety of materials (e. g. for the presently considered ensemble of six III-V materials), one would be concerned with the somewhat cumbersome circumstance that fitted magnitudes of the respective expansion coefficients, $r_n(T_s)$, are changing strongly (partly even by orders of magnitude) from one material to the other. Fortunately, such strong variations of parameter sets could throughout be avoided due to our adoption of different, material-specific values for the scaling temperatures, $T_s^{(fixed)} = T_h$ (due to Eq. (9)).

Taking further into account that, in the lower cryogenic regions (from 0 up to T_h, at least), the isobaric lattice heat capacities, $C_p(T)$, are nearly coincident with the harmonic parts of isobaric heat capacities, i. e. $C_p(0 < T \leq T_h) \cong C_{Vh}(0 < T \leq T_h)$, it follows readily from Eq. (10) (and Eq. (A2)) that $\kappa_P(T_h) \cong 0.5$. Observing further that the $\propto T^{-2n}$ terms in the numerator of Eq. (10) (as well as the $\propto T^{-14}$ term in the denominator) at the point $T \to T_h$ use to be by orders of magnitude smaller than unity, we see that the denominator at the point $T \to T_s = T_h$ must be approximately equal to 2. This corresponds to an approximate equality of

$$r_2(T_h) + \sum_{n=4}^{8} r_n(T_h) \cong 3, \tag{A4}$$

for the sum of the T_h-related expansion coefficients occurring in the denominator of Eq. (10).

APPENDIX B: DETERMINATION OF LIMITING DEBYE TEMPERATURES DUE TO THE HARMONIC REGIME

An effective procedure for determining high-temperature limiting Debye temperatures, $\Theta_{Dh}(T \to \infty)$ on the basis of measured (isobaric) low-temperature heat capacity data, $C_p(T) \to C_{Vh}(T)$, had been invented years ago by Barron *et al.*[29,31] A convenient feature of this conventional method is due to the circumstance that, in analogy to the exponential series analysis scheme,[82] it does not assume a preliminary analytical modeling of PDOS spectral functions. This method is based on the observation that the low-temperature dependences of squares, $(\Theta_{Dh}(T))^2$, of the "true" Debye temperatures, which are defined (in analogy to Eq. (20)) on the basis of the harmonic heat capacity components, $C_{Vh}(T)$ (Eq. (3)), can be generally represented in form of Taylor series expansions involving exclusively even-order powers of the reciprocal temperature with alternating signs,[29,31,43,47,50,97] i. e. explicitly

$$(\Theta_{Dh}(T))^2 = (\Theta_{Dh}(\infty))^2 \left(1 + \sum_{s=1}^{\infty} (-1)^s a_{2s} \left(\frac{\Theta_{Dh}(\infty)}{T}\right)^{2s}\right). \tag{B1}$$

Here $\Theta_{Dh}(\infty)$ represents the $T \to \infty$ limit of the "true" (harmonic) Debye temperature, and the expansion coefficients a_{2s} use to be positive (and are strongly decreasing in magnitude with increasing order, $1 \gg a_2 \gg a_4 \gg a_6 \ldots$; cf. Table V).

Furthermore, within the frame of the present study, we have found that in the vicinities of the maxima of the effective Debye temperatures, $\Theta_D(T) \approx \Theta_{D\,\max}$ (cf. Figs. 7 and 8 and Table III), where the differences $\Theta_{Dh}(T) - \Theta_D(T)$ between "true" and effective Debye temperatures are as a rule relatively small, $\Theta_{Dh}(T) - \Theta_D(T) \ll \Theta_{Dh}(T)$ (cf. also Figs. 12 and 13), these differences are in good approximation proportional to certain T^p-power dependences, $[\Theta_{Dh}(T) - \Theta_D(T)] \propto T^p$,

TABLE V. Limiting values of "true" (harmonic) Debye temperatures, $\Theta_{Dh}(\infty) \equiv \varepsilon_D^{\infty}/k_B$, and of the respective expansion coefficients involved by Eq. (B1), a_2 to a_8, which have been determined, in combination with the empirical parameters p and a_p, via fittings (see Figs. 12 and 13) of effective Debye temperatures, $\Theta_D(T)$, by means of Eq. (B2). Further quoted are the moment-related even-order phonon energies, $\varepsilon_P(m) \equiv (\mu_P^{(m)})^{1/m}$ ($m = 2$ to 10), which are resulting from Eqs. (B3a) to (B3e) for the corresponding moments, $\mu_P^{(m)}$.

	GaP	GaAs	GaSb	InP	InAs	InSb
intervals (K)	60 to 290	20 to 240	20 to 250	30 to 300	20 to 270	17 to 270
$\Theta_{Dh}(\infty)$((K)	522.3	375.6	308.2	448.5	314.9	250.6
$\varepsilon_{Dh}(\infty)$ ((meV)	45.0	32.4	26.6	38.6	27.1	21.6
a_2	1.178×10^{-2}	0.898×10^{-2}	1.102×10^{-2}	1.536×10^{-2}	1.211×10^{-2}	1.166×10^{-2}
a_4	1.005×10^{-4}	0.579×10^{-4}	0.868×10^{-4}	1.407×10^{-4}	0.964×10^{-4}	0.908×10^{-4}
a_6	0.415×10^{-6}	0.170×10^{-6}	0.334×10^{-6}	0.607×10^{-6}	0.370×10^{-6}	0.348×10^{-6}
a_8	0.654×10^{-9}	0.184×10^{-9}	0.494×10^{-9}	0.979×10^{-9}	0.540×10^{-9}	0.514×10^{-9}
p	3.287	3.210	2.958	2.034	4.396	3.744
a_p	0.519	0.246	0.376	0.085	0.218	0.863
$\varepsilon_P(2)$ (meV)	34.9	25.1	20.6	29.9	21.0	16.7
$\varepsilon_P(4)$ (meV)	39.1	27.7	23.0	34.2	23.6	18.7
$\varepsilon_P(6)$ (meV)	41.5	29.2	24.4	36.5	25.1	19.9
$\varepsilon_P(8)$ (meV)	43.2	30.3	25.3	38.0	26.1	20.7
$\varepsilon_P(10)$ (meV)	44.4	31.1	26.0	39.1	26.8	21.2

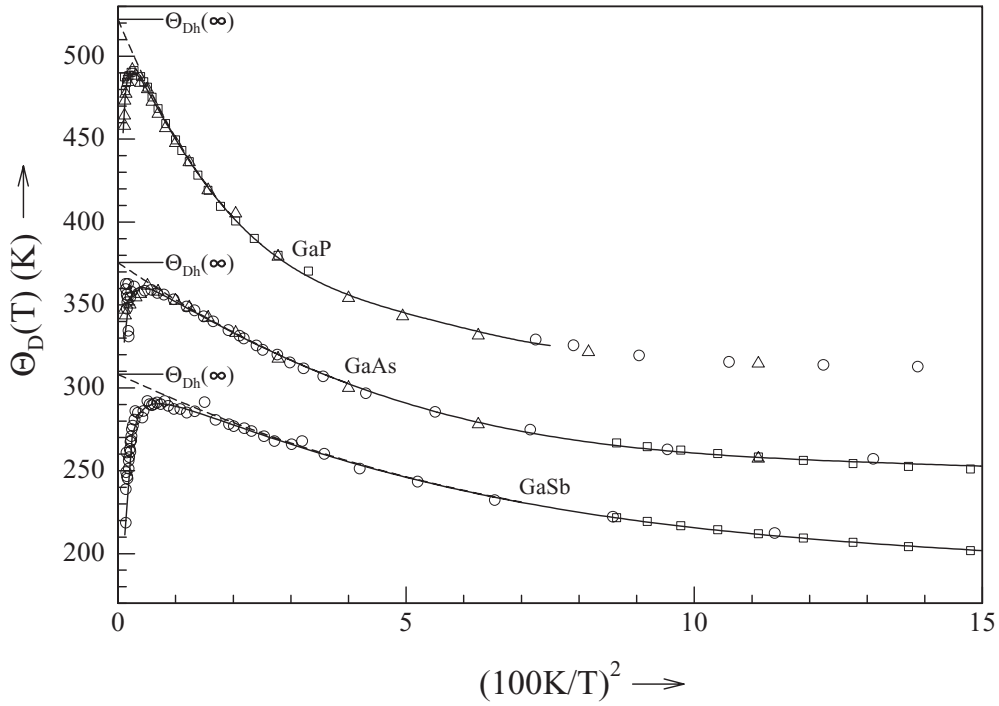

FIG. 12. $\Theta_D(T)$ vs. T^{-2} representation of effective Debye temperatures (cf. Fig. 7), which are due to the $C_p^{low}(T)$ data in consideration for GaP (Refs. 54 (○), 57 (△), and 91 (□)), for GaAs (Refs. 32 (□), 52 (○), and 58 (△)), and for GaSb (Refs. 32 (□) and 52 (○)). Solid curves are representing the fittings of the $\Theta_D(T)$ data by means of Eq. (B2), with the empirical parameter values quoted in Table V. Dashed curves show the corresponding high-temperature dependences of the "true" (harmonic) Debye temperatures, $\Theta_{Dh}(T)$ (due to Eq. (B1)).

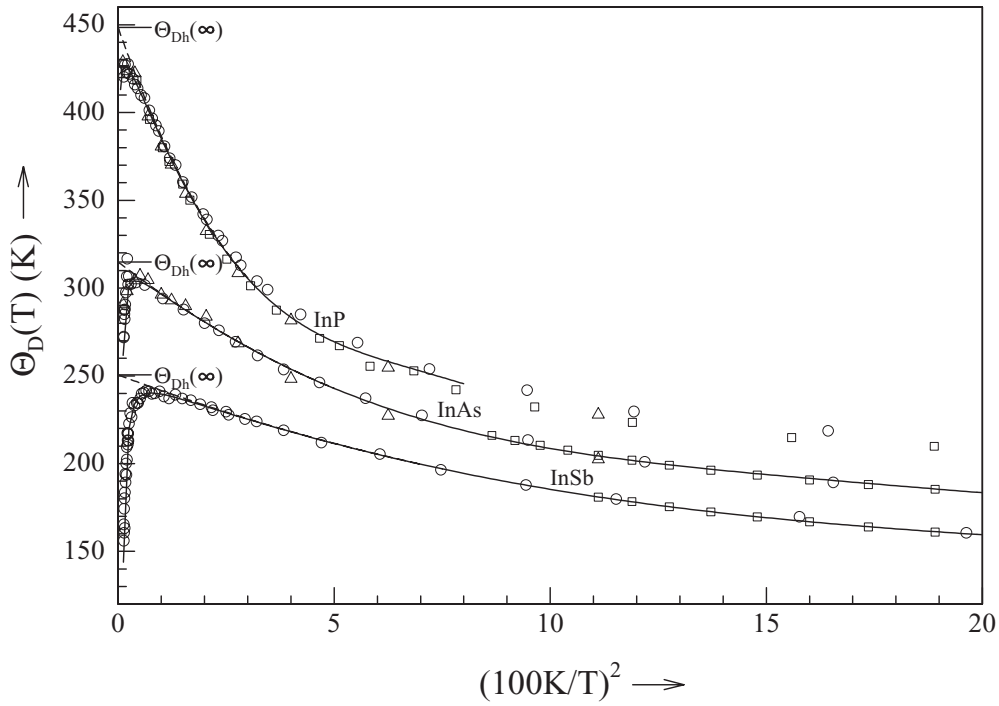

FIG. 13. $\Theta_D(T)$ vs. T^{-2} representation of effective Debye temperatures (cf. Fig. 8), which are due to the $C_p^{low}(T)$ data in consideration for InP (Refs. 52 (○), 60 (△), and 94 (□)), for InAs (Refs. 32 (□), 52 (○), and 60 (△)), and for InSb (Refs. 32 (□) and 52 (○)). Solid curves are representing the fittings of these $\Theta_D(T)$ data by means of Eq. (B2), with the empirical parameter values quoted in Table V. Dashed curves show the corresponding high-temperature dependences of the "true" (harmonic) Debye temperatures, $\Theta_{Dh}(T)$ (due to Eq. (B1)).

with exponents ranging usually within an interval of $2 < p < 5$. This means that the T-dependences of the effective Debye temperatures in these regions can be described approximately by an expression of the form

$$\Theta_D(T) \cong \Theta_{Dh}(\infty)\sqrt{\left(1+\sum_{s=1}^{\infty}(-1)^s a_{2s}\left(\frac{\Theta_{Dh}(\infty)}{T}\right)^{2s}\right)}\times\left[1-a_p\left(\frac{T}{\Theta_{Dh}(\infty)}\right)^{p}\right]. \qquad \text{(B2)}$$

Henceforth, we can determine the limiting Debye temperature, $\Theta_{Dh}(\infty)$, and the expansion coefficients, a_{2s} (s = 1, 2, 3, ...), in combination with the anharmonicity-related parameters p and a_p, via least-mean-square fittings of given $\Theta_D(T)$ data sets on the basis of Eq. (B2). In this way we come to the fitted $\Theta_D(T)$ curves (solid curves, in Figs. 12 and 13). The associated $\Theta_{Dh}(T)$ curves follow then readily from the square root of Eq. (B1) (dashed curves, in Figs. 12 and 13). This unprecedented procedure of fitting more extended (non-monotonic) $\Theta_D(T)$ data sets (via Eq. (B2)), instead of truncated (monotonic) sections of $\Theta_D(T) \to \Theta_{Dh}(T)$ (via Eq. (B1)), has the significant advantage that parameter uncertainties, which were usually caused by more or less arbitrary choices of the upper truncation points for the residual $\Theta_D(T) \to \Theta_{Dh}(T)$ data to be actually fitted, can be largely avoided. The parameter values resulting from this more comprehensive fitting procedure for the materials under study are listed in Table V.

It had been shown within the frame of a duly detailed analytical study[50] that the first five even-order moments of PDOS spectra, $\mu_P^{(2)}$ to $\mu_P^{(10)}$, can be represented in form of products of corresponding even-order powers of the limiting Debye energies, $\varepsilon_{Dh}(\infty) \equiv k_B\Theta_{Dh}(\infty)$, in combination with characteristic non-Debye factors that are defined in terms of the individual expansion coefficients a_2 to a_8 (listed in Table V). The respective even-order moments of material-specific PDOS

spectra are given (according to the supporting information to Ref. 50) by the following expressions:[43]

$$\mu_P^{(2)} = \frac{3}{5}(\varepsilon_{Dh}(\infty))^2, \tag{B3a}$$

$$\mu_P^{(4)} = \left[\frac{3}{7} + 12a_2\right](\varepsilon_{Dh}(\infty))^4, \tag{B3b}$$

$$\mu_P^{(6)} = \left[\frac{1}{3} + \frac{108}{5}a_2 + \frac{1512}{5}a_4\right](\varepsilon_{Dh}(\infty))^6, \tag{B3c}$$

$$\mu_P^{(8)} = \left[\frac{3}{11} + \frac{200}{7}a_2 + \frac{2160}{7}(2a_4 + (a_2)^2) + 8640a_6\right](\varepsilon_{Dh}(\infty))^8, \tag{B3d}$$

$$\mu_P^{(10)} = \left[\frac{3}{13} + \frac{168}{5}a_2 + 880(a_4 + (a_2)^2) + 19008(a_6 + a_2a_4) + 266112a_8\right](\varepsilon_{Dh}(\infty))^{10}. \tag{B3e}$$

Let us still note that the first three ones of these relations are equivalent to those ones given for $\mu_P^{(2)}$,$\mu_P^{(4)}$, and $\mu_P^{(6)}$, in Refs. 29 and 31, whereas the subsequent two ones, for $\mu_P^{(8)}$ and $\mu_P^{(10)}$, are due to a more comprehensive analytical study.[50] The respective, moment-related phonon energy values, $\varepsilon_P(2s) \equiv (\mu_P^{(2s)})^{1/2s}$, are listed in Table V.

[1] Y. S. Touloukian and E. H. Buyco, *Specific Heat of Nonmetallic Solids, Thermophysical Properties of Matter*, Vols. 4 and 5 (IFI/Plenum, New York-Washington, 1970).
[2] O. Madelung (ed.), *Landolt-Börnstein: Numerical Data and Functional Relationships in Science and Technology*, Group III, Vols. 17a/b, 22a/b, and 41a/b (Springer-Verlag, Berlin, 1982, 1989, 1999–2002).
[3] S. Adachi, *Handbook on Physical Properties of Semiconductors*, Vols. 1, 2, and 3 (Kluwer Academic Publishers, Boston, Dordrecht, New York, London, 2004).
[4] O. Knacke, O. Kubashewski, and K. Hesselmann, *Thermochemical Properties of Inorganic Substances* (Springer-Verlag, Berlin, Heidelberg, 1991)
[5] I. Barin, *Thermochemical Data of Pure Substances*, 3rd edition (VCH Verlagsgesellschaft mbH, Weinheim, New York, Basel, Cambridge, Tokyo, 1995).
[6] I. Hurtado and D. Neuschütz (eds.), Landolt-Börnstein, *Numerical Data and Functional Relationships in Science and Technology*, Group IV, Vol. **19**, *Thermodynamic Properties of Inorganic Materials*), Subvolume A, Parts 1–4 (Springer-Verlag, Berlin, Heidelberg, 1999).
[7] C. G. Maier and K. K. Kelley, J. Am. Chem. Soc. **54**, 3243 (1932)
[8] K. K. Kelley, U.S. Bureau of Mines, Bull. **584** (1960)
[9] L. B. Pankratz, Bureau of Mines (USA), Report of Investigations 6592 (1965)
[10] K. Yamaguchi, K. Itagaki, and A. Yazawa, J. Jpn. Inst. Metals **53**, 764 (1989)
[11] K. Itagaki and K. Yamaguchi, Thermochimica Acta **163**, 1 (1990)
[12] V. M. Glazov, A. S. Malkova, L. M. Pavlova, and A. S. Pashinkin, Russ. J. Phys. Chem. **74**, 145 (2000); [Zh. Fiz. Khimii **74**, 203 (2000)].
[13] V. M. Glazov, A. S. Malkova, and A. S. Pashinkin, Russ. J. Phys. Chem. **74**, 689 (2000); [Zh. Fiz. Khimii **74**, 789 (2000)].
[14] V. M. Glazov and A. S. Pashinkin, Inorg. Mater. **36**, 225 (2000); [Neorgan. Mater. **36**, 289 (2000).]
[15] A. S. Pashinkin and A. S. Malkova, Russ. J. Phys. Chem. **77**, 1889 (2003); [Zh. Fiz. Khimii **77**, 2097 (2003)].
[16] A. S. Pashinkin, A. S. Malkova, and M. S. Mikhailova, Russ. J. Phys. Chem. **83**, 1051 (2009); [Zh. Fiz. Khim. **83**, 1191 (2009)].
[17] A. S. Pashinkin, V. A. Fedorov, A. S. Malkova, and M. S. Mikhailova, Inorg. Mater. **46**, 1007 (2010); [Neorgan. Mater. **46**, 1121 (2010)].
[18] C. Chatillon, I. Ansara, A. Watson, and B. B. Argent, CALPHAD **14**, 203 (1990)
[19] R. H. Cox and M. J. Pool, J. Chem. Eng. Data **12**, 247 (1967)
[20] B. D. Lichter and P. Sommelet, Trans. Metall. Soc. AIME **245**, 1021 (1969).
[21] B. D. Lichter and P. Sommelet, Trans. Metall. Soc. AIME **245**, 99 (1969).
[22] A. Einstein, Ann. Phys. **22**, 180 (1907).
[23] P. Debye, Ann. Phys. **39**, 789 (1912).
[24] M. Blackman, in *Handbuch der Physik*, Band VI, Teil 1 (Springer-Verlag, Berlin-Göttingen-Heidelberg, 1955), p. 325.
[25] P. H. Keesom and N. Pearlman, in *Encyclopadia of Physics (Handbuch der Physik)*, vol. XIV: *Low temperature physics* I (*Kältephysik* I), ed. by S. Flügge (Springer-Verlag, Berlin-Göttingen-Heidelberg, 1956), p. 282.
[26] J. M. Ziman, *Electrons and Phonons* (Clarendon, Oxford, 1960).
[27] E. S. R. Gopal, *Specific Heats at Low Temperatures* (Plenum Press, New York, 1966).
[28] W. T. Berg and J. B. Morrison, Proc. Roy. Soc. A **242**, 467 (1957).

[29] T. H. K. Barron, W. T. Berg, and J. A. Morrison, Proc. Roy. Soc. A **242**, 478 (1957).
[30] T. H. K. Barron and J. A. Morrison, Proc. Roy. Soc. A **256**, 427 (1960).
[31] T. H. K. Barron, W. T. Berg, and J. A. Morrison, Proc. Roy. Soc. A **250**, 70 (1959).
[32] T. C. Cetas, C. R. Tilford, and C. A. Swenson, Phys. Rev. **174**, 835 (1968).
[33] M. Sanati, S. K. Estreicher, and M. Cardona, Solid State Commun. **131**, 229 (2004).
[34] M. Cardona, R. K. Kremer, M. Sanati, S. K. Estreicher, and T. R. Anthony, Solid State Commun. **133**, 465 (2005).
[35] A. Gibin, G. G. Devyatykh, A. V. Gusev, R. K. Kremer, M. Cardona, and H.-J. Pohl, Solid State Commun. **133**, 569 (2005).
[36] R. K. Kremer, M. Cardona, E. Schmitt, J. Blumm, S. K. Estreicher, M. Sanati, M. Boćkowski, I. Grzegory, T. Suski, and A. Jeżowski, Phys. Rev. B **72**, 075209 (2005).
[37] R. Pässler, J. Appl. Phys. **110**, 043530 (2011).
[38] S. N. Lykov and I. A. Chernik, Fiz. Tverd. Tela **24**, 3102 (1982).
[39] J. Serrano, R. K. Kremer, M. Cardona, G. Siegle, A. H. Romero, and R. Lauck, Phys. Rev. B **73**, 094303 (2006).
[40] M. Cardona, R. K. Kremer, R. Lauck, G. Siegle, J. Serrano, and A. H. Romero, Phys. Rev. B **76**, 075211 (2007).
[41] M. Cardona, R. K. Kremer, R. Lauck, G. Siegle, A. Muñoz, and A. H. Romero, Phys. Rev. B **80**, 195204 (2009).
[42] M. Cardona, R. K. Kremer, R. Lauk, G. Siegle, A. Muñoz, A. H. Romero, and A. Schindler, Phys. Rev. B **81**, 075207 (2010).
[43] R. Pässler, J. Phys. Chem. Solids **72**, 1296 (2011).
[44] R. K. Kremer, M. Cardona, R. Lauk, G. Siegle, and A. H. Romero, Phys. Rev. B **85**, 035208 (2012).
[45] R. Pässler, Phys. Status Solidi B **247**, 77 (2010).
[46] J. E. Desnoyers and J. A. Morrison, Phil. Mag. **3**, 42 (1958).
[47] P. Flubacher, A. J. Leadbetter, and J. A. Morrison, Phil. Mag. **4**, 273 (1959).
[48] G. Dolling and R. A. Cowley, Proc. Phys. Soc. (London) **88**, 463 (1966).
[49] W. Schnelle and E. Gmelin, J. Phys.: Condens. Matter **13**, 6087 (2001).
[50] R. Pässler, Phys. Status Solidi B **244**, 4605 (2007), including the supporting information (available in electronic form via http://www.wiley-vch.de/contents/jc_2232/2007/4605_s.pdf).
[51] U. Piesbergen, Z. Naturforsch. **18a**, 141 (1963).
[52] U. Piesbergen, Semiconductors and Semimetals **2**, 49 (1966).
[53] R. Banerjee and Y. P. Varshni, Can. J. Phys. **47**, 451 (1969).
[54] S. C. Abrahams and F. S. L. Hsu, J. Chem. Phys. **63**, 1162 (1975).
[55] M. K. Farr, J. G. Traylor, and S. K. Sinha, Phys. Rev. B **11**, 1587 (1975).
[56] M. Vandevyver and P. Plumelle, J. Phys. Chem. Solids **38**, 765 (1977).
[57] A. F. Demidenko, V. I. Koshchenko, A. S. Pashinkin, and V. E. Yachmenev, Inorg. Mater. **17**, 677 (1981); [Izv. Akad. Nauk SSSR Neorgan. Materialy **17**, 949 (1981)].
[58] N. N. Sirota, V. V. Novikov, and A. M. Antiukhov, "Doklady Akad. Nauk SSSR," Ser. Mat./Fiz. **263**, 96 (1982).
[59] N. N. Sirota, A. M. Antiukhov, V. V. Novikov, and A. A. Sidorov, "Doklady Akad. Nauk SSSR," Ser. Mat./Fiz. **266**, 105 (1982).
[60] N. N. Sirota, A. M. Antyukhov, V. V. Novikov, V. A. Fyodorov, Cryst. Res. Technol. **17**, 279 (1982).
[61] H. M. Kagaya and T. Soma, Phys. Status Solidi B **134**, K101 (1986).
[62] V. V. Novikov, Russ. J. Phys. Chem. **80**, 1456 (2006); [Zh. Fiz. Khim. **80**, 1645 (2006)].
[63] M. Born *Atomtheorie des festen Zustandes* (Teubner, Leipzig-Berlin, 1923).
[64] E. Grüneisen, in *Handbuch der Physik*, eds. H. Geiger and K. Scheel, Band X, *Thermische Eigenschaften der Stoffe* (Springer-Verlag, Berlin, 1926), p. 1.
[65] E. Schrödinger, in *Handbuch der Physik*, eds. H. Geiger and K. Scheel, Band X, *Thermische Eigenschaften der Stoffe* (Springer-Verlag, Berlin, 1926), p. 275.
[66] A. Euken, Wien-Harms Handbuch der Experimentalphysik, Bd. 6 (I) (1929).
[67] G. Leibfried and W. Brenig, Z. Phys. **134**, 451 (1953).
[68] A. F. Demidenko, V. I. Koshchenko, Z. S. Medvedeva, and A. F. Radchenko, "Izv. Akad Nauk SSSR," Neorg. Mater. **11**, 2117 (1975).
[69] A. D. Mah, E. G. King, W. W. Weller, and A. U. Christensen, Bur. Mines Rep. Invest. (USA) **RI-5716**, 1 (1961).
[70] B. A. Danilchenko, T. Paszkiewicz, S. Wolski, A. Jeżowski, and T. Plackowski, Appl. Phys. Lett. **89**, 061901 (2006).
[71] D. Sedmidubský and J. Leitner, J. Cryst. Growth **286**, 66 (2006).
[72] D. Sedmidubský, J. Leitner, P. Svoboda, Z. Sofer, and J. Macháček, J. Therm. Anal. Calorim. **95**, 403 (2009).
[73] P. Svoboda, D. Sedmidubský, and J. Leitner, Int. J. Mat. Res. (formerly Z. Metallkd.) **100**, 1246 (2009).
[74] R. Pässler, Phys. Status Solidi B **248**, 904 (2011) including a supporting information (available in electronic form via http://onlinelibrary.wiley.com/doi/10.1002/pssB201046248/suppinfo)
[75] P. Svoboda, P. Javorský, M. Diviš, V. Sechovský, F. Honda, G. Oomi, and A. A. Menovsky, Phys. Rev B **63**, 212408 (2001).
[76] W. N. Lawless and T. K. Gupta, J. Appl. Phys. **60**, 607 (1986).
[77] R. A. Slack, A. A. Maradudin, and G. H. Weiss, Phys. Rev. **124**, 717 (1961).
[78] A. A. Maradudin and R. F. Wallis, Phys. Rev. **148**, 945 (1966).
[79] L. J. Porter, J. Li, and S. Yip, J. Nuclear Mat. **246**, 53 (1997).
[80] H. Neumann, Cryst. Res. Technol. **39**, 245 (2004).
[81] H. Neumann, J. Łażevski, P. T. Jochym, and K. Parlinski, Phys. Rev. B **75**, 224301 (2007).
[82] R. Pässler, Phys. Status Solidi B **245**, 1133 (2008).
[83] R. Pässler, Phys. Status Solidi B **243**, 2719 (2006).
[84] R. Pässler, J. Appl. Phys. **101**, 093513 (2007).
[85] H. Thirring, Phys. Z. **14**, 867 (1913); **15**, 180 (1914).
[86] J. C. Holste, Phys. Rev. B **6**, 2495 (1972).

[87] G. K. White and S. J. Collocott, J. Phys. Chem. Ref. Data **13**, 1251 (1984).
[88] T. H. K. Barron and G. K. White, *Heat Capacity and Thermal Expansion at Low Temperatures* (Kluwer Academic / Plenum Publishers, New York, 1999).
[89] S. Sönmezoğlu, Int. J. Mod. Phys. **22**, 5349 (2008).
[90] B. A. Mamedov, E. Eser, H. Koç, and I. M. Askerov, Int. J. Thermophys. **30**, 1048 (2009).
[91] V. V. Tarassov and B. F. Demidenko, Phys. Status Solidi B **30**, 147 (1968).
[92] H. Neumann, G. Kühn, and W. Möller, Phys. Status Solidi B **144**, 565 (1987).
[93] B. J. Dash, B. Finch, and P. J. Gardner, J. Chem. Eng. Data **19**, 113 (1974).
[94] V. Novikov, Ph. D. thesis, Univ. of Bryansk, Russia, 1984.
[95] M. Ahrens and J. Maier, Thermochimica Acta **443**, 189 (2006).
[96] I. Zięborak-Tomaszkiewicz, R. Świerzewski, and P. Gierycz, J. Therm. Anal. Calorim. **91**, 649 (2008).
[97] U. C. Boehnke, G. Kühn, F. I. Frolova, I. E. Paukov, and H. Neumann, J. Therm. Analysis **33**, 205 (1988).